Evaluation of the Prediction Capability of AHP and F_AHP Methods in Flood Susceptibility Mapping of Ernakulam District (India)

RESHMA VILASAN (reshmavilasan@gmail.com)
Visvesvaraya National Institute of Technology https://orcid.org/0000-0002-6401-1548
Vijay S Kapse
Visvesvaraya National Institute of Technology

Research Article

Keywords: Analytical hierarchy process, Flood susceptible zones, Fuzzy-AHP, GIS

Posted Date: June 29th, 2021

DOI: https://doi.org/10.21203/rs.3.rs-655658/v1

Version of Record: A version of this preprint was published at Natural Hazards on March 9th, 2022. See the published version at https://doi.org/10.1007/s11069-022-05248-4.

Evaluation of the prediction capability of AHP and F_AHP methods in flood susceptibility mapping of Ernakulam district (India)

Reshma T Vilasan [1], Vijay S Kapse [2]

[1] Ph.D. Scholar, Visvesvaraya National Institute of Technology, Nagpur, India
[2] Head of Department, Visvesvaraya National Institute of Technology, Nagpur, India

Abstract

Floods are one of the frequent natural hazards occurring in Kerala because of the remarkably high annual rate of rainfall. The objective of this study is to prepare the flood susceptibility maps of the Ernakulam district by integrating remote sensing data, GIS, and analytical hierarchy process (AHP), and fuzzy-analytical hierarchy process methods. Factors such as slope angle, soil types (texture), land use/land cover, stream density, water ratio index, normalized difference built-up index, topographic wetness index, stream power index, aspect, sediment transport index have been selected. The area of the final maps is grouped into five flood susceptible zones, ranging from very low to very high. The major reasons for flood occurrence in Ernakulam district are the combined effect of multiple factors such as excess silting, reduction of stream width due to human intervention, and changes in land cover and land use pattern, lower slope, higher soil moisture content, lower stream capacity, and poor infiltration capacity of soils. The prepared map was validated using the receiver operating characteristic (ROC) curve method. The area under the ROC curve (AUC) values of 0.75 and 0.81 estimated by the ROC curve method for the AHP and F-AHP methods is considered acceptable and excellent, which confirms the prediction capability of the prepared maps. The very high susceptible zone constitutes around 19% of the district. This map is useful for land-use planners and policymakers to adopt strategies which will reduce the impact of flood hazard and damage in the future.

Keywords: *Analytical hierarchy process, Flood susceptible zones, Fuzzy-AHP, GIS*

1. Introduction

Flooding is one of the natural hazards that often cause significant damage to property and loss of life (Merkuryeva et al. 2015). This condition can arise from diverse hydrological processes, such as high tide levels, precipitation, high groundwater levels, and high river flows (Acreman and Holden 2013). Fluvial floods can be defined as the overflowing of streams or other water bodies of accumulated water over areas that are not normally inundated with water (Pratomo et al. 2016). The frequency of flooding is expected to increase due to unscientific modifications of drainage channels and unplanned development in the drainage basin because of urbanization, deforestation, and prolonged rainfall (Tehrany et al. 2015). Fluvial floods can occur due to the clogging of river channels because of sedimentation (Martín-Vide et al. 2014), snowmelt, or, in rare cases, dam collapse (Acreman and Holden 2013). Multiple factors, including heavy rainfall, poor infiltration capability of the soil, climate change, changes in land-use patterns, can lead to flooding (Ali et al. 2020). Floods can cause infrastructure losses (transportation networks, communication networks, etc.), residential losses, public facilities losses, and agricultural losses (damages to land, productivity, crop loss), and impact on water quality, accessibility, and availability (Petersen 2001; Smiley and Hambati 2019). Drowning, electrical injuries, and hypothermia are the direct health consequences, while indirect health effects include displacement of populations, intermittent disruption of public health services, lower income, and insufficient temporary living conditions (Allaire 2018).

Flooding can cause mortality, injuries, mental disorder, and transmission of fecal-oral diseases (Cholera, Cryptosporidiosis, Diarrhea, Poliomyelitis, Rotavirus, Typhoid, Paratyphoid, etc.), rodent-borne diseases (Hantavirus pulmonary syndrome, Leptospirosis, etc.), vector-borne diseases (Malaria, Lymphatic filariasis, and Arbovirus disease) (Ahern et al. 2005).

Flooding is one of the frequently occurring natural hazards in India. India is one of the worst-affected countries in the world after Bangladesh (Panda and Sahoo 2015). About 40 million hectares (almost 12% of the area) of India are susceptible to floods (Husain 2012). India receives 75% of the rain during the S-W monsoon season (June–September) (Agnihotri and Mohapatra 2012). Most of the rivers overflow during this period, resulting in intense recurring floods. The devastating floods of 2018 and 2019 caused significant damage to infrastructure, property and resulted in hundreds of deaths in Kerala (Mishra and Shah 2018; Government of Kerala 2019; Hunt and Menon 2020). The flood-hit Kerala faced diseases such as Chikungunya, Dengue, Cholera, Typhoid, Hepatitis, and Leptospirosis (Jobin and Prakash 2020). Leptospirosis has long been a major threat to Kerala with more than 1000 cases reported annually (James et al. 2018). By providing the public with accurate information on flood risk through flood susceptibility maps, the damages and losses can be minimized.

Remote sensing (RS) and GIS have made significant contributions in disaster management studies such as those related to floods (Brivio et al. 2002; Dewan et al. 2006; Fernández and Lutz 2010; Paquette and Lowry 2012; Ajin et al. 2013; Tiryaki and Karaca 2018; Ajin et al. 2019; Ullah and Zhang 2020; Msabi and Makonyo 2021), droughts (Krishna et al. 2009; Muthumanickam et al. 2011; Belal et al. 2014; Legesse and Suryabhagavan 2014; Dutta et al. 2015; Orimoloye et al. 2019), forest fires (Adab et al. 2013; Ajin et al. 2018; Jaiswal et al. 2002; Abedi Gheshlaghi 2019; Bentekhici et al. 2020; Parajuli et al. 2020), landslides (Shahabi and Hashim 2015; Ajin et al. 2016; Anis et al. 2019; Berhane et al. 2020). The AHP method has been effectively used by many researchers (Rahman et al. 2019; Vojtek and Vojteková 2019; Das 2020; Domakinis et al. 2020; Souissi et al. 2020; Swain et al. 2020) to demarcate flood susceptible zones. While researchers like Bouamrane et al. (2020) and Kumi-Boateng et al. (2020) used both AHP and F-AHP methods to delineate flood susceptible zones. The objectives of this study are to delineate the flood susceptible zones in the Ernakulam district by integrating RS data and GIS, to compare the prediction capability of both AHP and F-AHP methods, to understand and analyze the recent induced reasons for the occurrence of floods. Ten causative factors, namely slope angle, soil types (texture), land use/land cover (LULC), stream density, water ratio index (WRI), normalized difference built-up index (NDBI), topographic wetness index (TWI), stream power index (SPI), slope aspect, and sediment transport index (STI) have been selected for the mapping process.

3. Materials and methods

3.1. Study area

The study area, Ernakulam district is situated almost in the middle of Kerala State and on the coast of the Arabian Sea. The district lies between the longitude of 76° 16' 48.00" and latitude of 9° 58' 48.00" N and spans an area of about 3068 Sq.Km (Figure 1). The district is bounded on the North by Thrissur District, on the south by Kottayam and Alappuzha Districts, and on the east by Idukki district and the Arabian Sea lies all along the western boundary of the District. The climate in the area is tropical humid, with a long hot season and plenty of seasonal rainfall. A part of the Western Ghats forms the hilly tract along the eastern portion. Figure 1 shows the location of the study

area. The district receives on an average 3450 mm of annual rainfall. South-west monsoon contributes about 67.4% to annual rainfall. About 30 percent of the area is urban where about 49 percent of the district's population live (Census, 2011).

3.2. Data source

The Ernakulam district is covered by topographic maps numbered 58 B/4, 58 B/7, 58 B/8, 58 B/11, 58 B/12, 58 B/15, 58 B/16, 58 C/1, 58 C/5, 58 C/9, 58 F/3, 58 F/4 at a scale of 1:50,000. The data used in this study include SoI topographic maps, Landsat 8 OLI (Operational land imager) satellite images of 30 m spatial resolution, SRTM (Shuttle radar topography mission) DEM (Digital elevation model) of 30 m spatial resolution, and soil data collected from the Kerala State Land Use Board (KSLUB) at 1:250,000 scale. After projecting the data to Universal Transverse Mercator (WGS 84; 43N), the thematic map layers of the factors such as slope, soil, land use/land cover, stream density, WRI, NDBI, TWI, SPI, aspect, and STI were generated using ESRI ArcGIS 10.8 and ERDAS Imagine 8.4 software tools. The map layers of factors such as slope, stream density, WRI, NDBI, TWI, SPI, aspect, and STI were classified using the natural breaks (Jenks) classification method (Mersha and Meten 2020; Ahmadlou et al. 2021). The thematic map layers were resampled to 30 m×30 m pixel size and the flood susceptibility maps were created using ArcGIS (Map algebra) tools after assigning the AHP and F-AHP weights. The AHP weights were computed using Microsoft Excel and the F-AHP weights were determined using FisPro 3.7. The flood susceptibility maps were validated using the flood inundation data of the years 2013, 2018 and 2019 collected from the records of the National Remote Sensing Centre (NRSC), Hyderabad, India. The ROC curves were plotted using the RStudio software to validate the prepared susceptibility maps.

3.3. Causative factors

Slope angle

The rate of infiltration and volume of water retention decreases with an increase in slope (Tehrany et al. 2017). The slope of the study area was derived from the SRTM DEM using ArcGIS spatial analyst tools. The slope angle of the Ernakulam district has been classified into five classes including, 0 – 5.00, 5.00 – 11.88, 11.88 – 21.26, 21.26 – 33.46, and 33.46 – 79.75 (Figure 2). In this district, areas most seriously affected by floods have lower slope values (0 – 5.00°).

Soil types

Soil types are important as far as the vulnerability to flooding of an area is concerned. Soils with lower porosity have less pore spaces and hence a lower infiltration rate, and the decrease in infiltration leads to higher runoff and greater flooding potential (Gregory et al. 2016). The steady-state infiltration rate of sand, loam, and clay are > 0.8 in/hr, 0.2-0.4in/hr, and 0.04-0.2 in/hr respectively (Hillel 1982). The infiltration during rainfall events is controlled by hydraulic conductivity, and because of larger pores, sandy soil has higher hydraulic conductivity than fine-textured soils (Prachansri 2017). As a result, areas with clayey soil are more prone to flooding. The soil layer was digitized from the soil map published by KSLUB in ESRI ArcGIS 10.6. In general, five different types of soil are observed (Figure 3) as clay, gravelly clay, loam, gravelly loam, and sand.

LULC

The land cover of a region is usually classified based on the amount and type of vegetation, which reflects its use, environment, cultivation, and seasonal phenology (El Morjani et al. 2017). The urban and industrial areas have been subjected to topographic modification due to human intervention. These areas are mainly made of impervious surfaces such as buildings and roads, which reduce the volume of water naturally available for infiltration and hence increase the volume of overland flow causing floods (Gigović et al. 2017). Built-up areas obstruct natural drainage, leading to flooding. The land use and land cover types were derived from the Landsat 8 OLI satellite image acquired in the year 2020 using ERDAS Imagine software. The maximum likelihood classifier (Ayele et al. 2018; Alam et al. 2020) was used to classify the different land use/land cover types of the district. The land use/land cover types of the district are deciduous forest, evergreen forest, scrubland, barren land, built-up area, agricultural land, wetland, mixed vegetation, and water body (Figure 4). In the present study, the flood-affected areas are intensely cultivated terrains, especially the paddy fields, and hence, the loss of agricultural land and related economic losses will be remarkably high.

Stream density

Stream densities are closely linked to various hydrological processes such as infiltration, saturation of the soil, sheet erosion, overland flows, and the interactions between them to regulate sediment and runoff (Moglen et al. 1998). However, higher stream density need not imply a higher rate of runoff. This is because the stream capacity depends on the width, depth, and length of drainage channels. In the study area, the distributaries of the mainstream are narrow, tortuous, and shallow. Therefore, water retention leads to flooding. In addition to this, the existing narrow stream channels in the lower parts of the study area are partially blocked due to heavy silting. This explains the frequent flooding of the lower stretches of the Ernakulam district. The stream networks were digitized from the SoI topographic maps and the stream density layer was prepared using ArcGIS spatial analyst tools. The stream density of the study area is grouped into five classes (Figure 5). They are 0–1.47 km/km^2, 1.47–3.17 km/km^2, 3.17–6.02 km/km^2, 6.02–12.78 km/km^2, and 12.78–26.94 km/km^2.

WRI

WRI of the Ernakulam district was derived from the Landsat 8 OLI images using Equation 1 (Shen and Li 2010) and ArcGIS tools.

$$\mathrm{WRI} = \frac{(\mathrm{Green}+\mathrm{Red})}{(\mathrm{NIR}+\mathrm{SWIR})} \quad (1)$$

The WRI value above 1 represents water (Shen and Li 2010). The WRI of the study area ranges between 0.26 and 1.42 (Figure 6) and is categorized into five classes (0.26-0.46, 0.46-0.56, 0.56-0.70, 0.70-0.98, and 0.98-1.42). The chance of flooding is high in areas with higher WRI.

NDBI

NDBI is a satellite-derived index that represents urban built-up areas (Bhatti and Tripathi 2014). The NDBI value close to 0 represents woodland, the NDBI value less than 0 represents a body of water, and the NDBI value greater than 0 represents built-up areas (Zha et al. 2003). NDBI was extracted using Equation 2 (Shahfahad et al. 2020) and ArcGIS spatial analyst tools.

$$\mathrm{NDBI} = \frac{\mathrm{SWIR}-\mathrm{NIR}}{\mathrm{SWIR}+\mathrm{NIR}} \quad (2)$$

NDBI of Ernakulam district is grouped into five classes: -0.43 - -0.21, -0.21 – -0.14, -0.14 – -0.07, -0.07 – 0.00, and 0.00 – 0.43 (Figure 7). The chance of flooding is high in areas with higher NDBI.

TWI

TWI represents the soil moisture content and surface saturation (Yong et al. 2012). Higher soil moisture content and soil saturation favour flooding (Ho-Hagemann et al. 2015). When the saturation level increases, the local groundwater table rises. Eventually, the zone of aeration becomes fully saturated, setting the condition for flooding. Therefore, the areas with higher TWI are more prone to flooding. The TWI of the study area was derived from the SRTM DEM. TWI was computed using Equation 3 (Beven and Kirkby 1979) and spatial analyst tools with ArcGIS software.

$$\mathrm{TWI} = \ln(\alpha/\tan\beta) \quad (3)$$

Where α is the specific catchment area (A = *A*/*L*, catchment area (*A*) divided by contour length (*L*)] and β is the local slope

The present study has classified the district into 5 classes (0.61–6.82, 6.82–19.38, 19.38–41.61, 41.61–80.26, and 80.26–246.45) based on TWI as shown in Figure 8. This study confirms the fact that the areas affected by frequent floods in the study area are characterized by the highest TWI (80.26-246.45).

SPI

SPI is the water flow power in terms of erosion (Altin and Gökkaya 2015). It determines the capacity of a river to carry sediment (Bizzi and Lerner 2015). In the upstream segment, because of higher stream power, the streams can erode and transport a significant volume of debris. The channels become shallow and meandering when the stream power is declined, resulting in overbank deposition of sediment (Graf 1983). This is a major reason for flooding on the lower plains. The SPI was derived from the SRTM-DEM. SPI was calculated using Equation 4 (Moore et al. 1991).

$$\mathrm{SPI} = \alpha \tan \beta \quad (4)$$

Where α is the specific catchment area (A = *A*/*L*, catchment area (*A*) divided by contour length (*L*)] and β is the local slope.

The present study has classified the Ernakulam district into 5 classes (-38.15 – -5.19, -5.19 – -2.08, -2.08 – -0.65, -0.65 – 0.29, and 0.29 – 22.75) based on the stream power index as shown in the map (Figure 9). It was found that most of the flood-affected areas have the lowest SPI (-38.15 – -5.19).

Slope aspect

The slope aspect (Figure 10) of the study area was prepared from the SRTM DEM using ArcGIS spatial analyst tools and has been grouped into nine classes (Flat, North, Northeast, East, Southeast, South, Southwest, West, and Northwest). Because of the rapid accumulation of water, flooding is more likely in areas with flat aspects. The

184 southern and western aspects will be drier and less prone to flooding, as there are greater solar and wind influences
185 in the southern aspects and a higher heating intensity in the western aspects (Setiawan et al. 2004).

186 **STI**

187 STI refers to sediment movement caused by water flow (Tehrany et al. 2019). STI characterizes erosion and
188 deposition processes (Kalantari et al. 2014; Kumar and Gupta 2016). The high STI reflects the erosion process,
189 whereas the low STI reflects the deposition process. STI was derived from the SRTM DEM using Eq. 5 (Moore
190 et al. 1993) and ArcGIS spatial analyst tools.

191 $$\mathrm{STI} = \left(\frac{\alpha}{22.13}\right)^{0.6}\left(\frac{\sin\beta}{0.0896}\right)^{1.3} \quad (5)$$

192 Where α is the area of the catchment (m^2) and β (radians) is the slope gradient.

193 The STI of the study area ranges from 0 to 247.77 and is grouped into 5 classes (Figure 11). The chance of flooding
194 will be high in areas with low SPI values, as these as depositional zones. The carrying capacity of stream channels
195 in these zones will be much reduced due to the deposition of sediments.

196 ## 3.4. The AHP modelling

197 AHP is the most used decision-making method developed by Saaty (1980) to solve complex decision problems.
198 By reducing complicated decisions to a number of pairwise comparisons, AHP helps to make the right decision
199 and calculates the results (Dekrita et al. 2019). For constructing judgement matrices, a 1-9 scale is used. The
200 important steps involved in AHP are the development of a pairwise comparison matrix, calculation of Eigen value,
201 Eigen vector and weighting coefficient (Table 1), and finally, calculation of consistency ratio to check the
202 consistency (Table 2).

203 **INSERT TABLE 1 HERE**

204 Where Slp. = Slope angle; SD = Stream density, Asp. = Slope aspect

205 The eigen vector (Vp), and weighting coefficient (Cp) were computed using Equations 6 and 7 (Danumah et al.
206 2016)

207 $$\mathrm{Vp} = \sqrt[k]{W1 \times \ldots Wk} \quad (6)$$

208 Where k = number of factors and W = ratings of the factors

209 $$\mathrm{Cp} = \frac{Vp}{Vp1 + \ldots\ldots Vpk} \quad (7)$$

210 **INSERT TABLE 2 HERE**

211 The eigen value (λ max), consistency index (CI), and consistency ratio (CR) were computed using Equations 8,
212 9, and 10 (Danumah et al. 2016)

213 $$\lambda\ \mathrm{max} = \frac{[E]}{k} \quad (8)$$

$$CI = (\lambda \max - k)/(k - 1) \quad (9)$$

$$CR = \frac{CI}{RI} \quad (10)$$

Where RI is the random index

Table 3 Random index (Saaty 1980)

Number of criteria	2	3	4	5	6	7	8	9	10	11
RI	0.00	0.58	0.90	1.12	1.24	1.32	1.41	1.45	1.49	1.51

The CR should be less than 0.1 (i.e., 10%) (Saaty 1980), otherwise, the judgements are untrustworthy and need to revise the subjective judgements. In this study, the CR is 0.041 (which is less than 0.1), hence the judgements are acceptable.

The final weights obtained through the AHP model are shown in Equation 11.

$$FSZ = (0.291 \times \text{Slp.}) + (0.216 \times \text{Soil}) + (0.155 \times \text{LULC}) + (0.110 \times \text{SD}) + (0.077 \times \text{WRI}) + (0.054 \times \text{NDBI}) + (0.038 \times \text{TWI}) + (0.027 \times \text{SPI}) + (0.019 \times \text{Asp.}) + (0.014 \times \text{STI}) \quad (11)$$

3.5. The Fuzzy-AHP modelling

F-AHP is an AHP approach developed utilizing the theory of fuzzy logic (Putra et al. 2018). The fuzzy approach that represents uncertainty in human judgements together with the AHP method can be used to provide more precise, specific, and realistic outcomes (Kaya et al. 2020; Lin 2020). In this study, the Buckley (1985) technique was followed by comparing the fuzzy ratios described as triangular membership functions. The major processes involved are the construction of pair-wise comparison of factors (Table 4), calculation of the geometric means of fuzzy comparison values (Table 5), relative fuzzy weights of each factor (Table 6), and averaged and normalized relative weights of factor (Table 7). The various steps involved with the F-AHP modelling are as follows:

Step 1: Comparison of the factors or alternatives by decision-makers

For example: if the decision-maker states that factor 1 (P1) is weakly significant than factor 2 (P2), then the fuzzy triangular scale will be (2, 3, 4). In the pair-wise contribution matrix of the factor for comparison of P2 to P1, the fuzzy triangular scale will be (1/4, 1/3, 1/2) (Ayhan 2013).

The pair-wise contribution matrix is depicted in Eq. 12.

$$\tilde{A}^k = \begin{bmatrix} \tilde{d}_{11}^k & \tilde{d}_{12}^k & \dots & \tilde{d}_{1n}^k \\ \tilde{d}_{21}^k & \dots & \dots & \tilde{d}_{2n}^k \\ \dots & \dots & \dots & \dots \\ \tilde{d}_{n1}^k & \tilde{d}_{n2}^k & \dots & \tilde{d}_{mn}^k \end{bmatrix} \quad (12)$$

Where $\tilde{d}_{ij}^k$ indicates the k[th] decision maker's preference of i[th] factor over j[th] factor (Ayhan 2013).

Step 2: When there is more than one decision-maker, the preferences ($\tilde{d}_{ij}^{k}$) are averaged, and ($\tilde{d}_{ij}$) is determined using Eq. 13.

$$\tilde{d}_{ij} = \frac{\sum_{k=1}^{K} \tilde{d}_{ij}^{k}}{K} \tag{13}$$

Step 3: The pair-wise comparison matrix is modified based on the averaged preferences using Eq. 14.

$$\tilde{A} = \begin{bmatrix} \tilde{d}_{11} & \cdots & \tilde{d}_{1n} \\ \vdots & \ddots & \vdots \\ \tilde{d}_{n1} & \cdots & \tilde{d}_{nn} \end{bmatrix} \tag{14}$$

INSERT TABLE 4 HERE

Step 4: The geometric average of fuzzy comparative values for each factor was determined using Eq. 15 (Buckley 1985).

$$\tilde{r}_i = \left(\prod_{j=1}^{n} \tilde{d}_{ij} \right)^{1/n}, \quad i = 1, 2, ..., n \tag{15}$$

Where $\tilde{r}_i$ still depicts the triangular values.

Step 5: From the next 3 sub-steps, the fuzzy weight of each factor was computed.

Step 5a: The vector summation of each $\tilde{r}_i$ was determined.

Step 5b: The (-1) power of the summation vector was computed, and the fuzzy triangular number was replaced, to convert it into increasing order.

INSERT TABLE 5 HERE

Step 5c: To compute the fuzzy weight of factors $i(\tilde{w}_i)_i$, each $\tilde{r}_i$ was multiplied with the reverse vector as in Eq. 16.

$$\begin{aligned} \tilde{w}_i &= \tilde{r}_i \otimes (\tilde{r}_1 \oplus \tilde{r}_2 \oplus ... \oplus \tilde{r}_n)^{-1} \\ &= (lw_i, mw_i, uw_i) \end{aligned} \tag{16}$$

INSERT TABLE 6 HERE

Step 6: The fuzzy weights were de-fuzzified using Eq. 17 (Chou and Chang 2008).

$$M_i = \frac{lw_i, mw_i, uw_i}{3} \tag{17}$$

Step 7: The Mi was standardized using Eq. 18.

$$N_i = \frac{M_i}{\sum_{i=1}^{n} M_i} \quad (18)$$

INSERT TABLE 7 HERE

The final weights obtained from the F-AHP modelling are shown in Equation 19.

$$\text{FSZ} = (0.282 \times \text{Slp.}) + (0.215 \times \text{Soil}) + (0.158 \times \text{LULC}) + (0.112 \times \text{SD}) + (0.078 \times \text{WRI}) + (0.055 \times \text{NDBI}) + (0.038 \times \text{TWI}) + (0.027 \times \text{SPI}) + (0.019 \times \text{Asp.}) + (0.014 \times \text{STI}) \quad (19)$$

3.6. Validation of the flood susceptibility maps

Finally, the flood susceptible zone map was validated using the flood inundation data provided by NRSC for the years 2013, 2018, and 2019. For the validation of the result, 570 locations within the flood inundated area were randomly selected (Figure 12). The receiver operating characteristic (ROC) curve analysis was performed using RStudio software to assess the prediction accuracy of the susceptibility map. When the area under ROC (AUC) equals 0.5, it indicates random chance and indicates perfect accuracy when AUC equals 1.0 (Zou et al. 2007). According to Hosmer and Lemeshow (2000), the AUC values are considered outstanding, excellent, and acceptable for values between 0.9-1.0, 0.8-0.9, and 0.7-0.8.

4. Results and discussion

The map layers of slope angle, soil, LULC, stream density, WRI, NDBI, TWI, SPI, aspect, and STI were combined using ArcGIS tools to prepare the flood susceptibility maps of the study area. The flood susceptibility maps were prepared using the weights derived by the AHP and F-AHP methods. The area of the flood susceptibility maps has been grouped into five classes, namely very low, low, moderate, high, and very high (Figure 13 and 14). The high and very high susceptible zones are located in the western parts of the study area. This area has a low slope, poor or very poorly drained soil, higher built-up developments, lower stream density, and high soil moisture content (WRI and TWI). The studies by Sarkar and Mondal (2020), Ullah and Zhang (2020) also found that high flood-prone areas are situated in areas with lower slopes and higher TWI. Like the findings of this study, Samanta et al. (2018) also found that the high and very flood susceptible zones are characterized by soils with poor to very poor drainage capacity. Ghosh and Mistri (2015) found that the reduced carrying capacity of stream channels due to excess siltation and drainage congestion is the major reason for flooding in the Damodar river basin. In their study, Erena and Worku (2018) also found that changes in the land use/land cover and encroachments of settlements (development activities) on the riverbank are the major reasons for flood risk. Bohorquez and del Moral-Erencia (2017) found vegetation encroachment as one of the major reasons for reduced stream channel capacity. The present study confirms that the flood occurring in this basin is due to the combined effect of natural factors, human intervention, and negligence in taking preventive measures. The area and percentage of each flood susceptible zone are shown in Table 8. The AUC values of 0.75 and 0.81 estimated by the ROC curve method confirm that the result is acceptable and excellent for the AHP and F-AHP modelling, respectively (Figure 15). This finding confirms that the F-AHP method is more effective in predicting flood-prone zones and was thus chosen as the best model. According to the F-AHP model, the very high susceptible zone covers 19.37% of the study area.

296 **Table 8** Area and percentage of flood susceptible zones

Susceptible Zones	AHP method		F-AHP method	
	Area of susceptible zones (Sq. km)	Percentage of the area of the flood susceptible zones	Area of susceptible zones (Sq. km)	Percentage of the area of the flood susceptible zones
Very low	267.18	11.10	267.66	11.12
Low	395.23	16.42	401.25	16.67
Moderate	643.87	26.75	662.16	27.51
High	623.41	25.90	609.69	25.33
Very high	477.31	19.83	466.24	19.37
Total	**2407**	**100**	**2407**	**100**

297 ## 5. Conclusions

298 Floods are one of the most common natural hazards occurring in the Ernakulam district and result in serious
299 damage to agriculture, infrastructure, and human and animal habitats. This study applied GIS techniques, and
300 AHP and F-AHP methods to prepare the flood susceptibility maps of the Ernakulam district. Floods occurring in
301 this district are the result of natural factors such as low slope gradient, lower capacity of stream channels, higher
302 soil moisture content, and poor infiltration capacity of soils, together with anthropogenic activities like blocking
303 the natural stream channels for construction purposes. An excellent AUC value of 0.81 obtained by the ROC curve
304 analysis for F-AHP proves the efficiency of the F-AHP method over the AHP method. The study confirms that
305 around 19.37% of the basin falls under a very high susceptible zone. The present study demonstrated an effective
306 model that can be used to delineate the flood susceptible zones, and this will help the land-use planners and
307 policymakers to implement policies that can help mitigate flood risk and damage in the future.

308 **Ethics declarations**

309 **Ethics Approval and Consent to Participate -** This article does not contain any studies with human participants
310 or animals performed by any of the authors. Informed consent is not applicable.

311 **Conflict of Interest / Competing interests -** The authors declare that they have no known competing financial
312 interests or personal relationships that could have appeared to influence the work reported in this paper.

313 **Availability of data and materials** - Not applicable.

314 **Financial interests** - All authors certify that they have no affiliations with or involvement in any organization or
315 entity with any financial interest or non-financial interest in the subject matter or materials discussed in this
316 manuscript.

317 **Author contributions -** All the authors made significant contributions to the manuscript. All authors read and
318 approved the final manuscript.

319

320

321

References

Abedi Gheshlaghi H (2019) Using GIS to develop a model for forest fire risk mapping. Journal of the Indian Society of Remote Sensing 47: 1173-1185. https://doi.org/10.1007/s12524-019-00981-z

Acreman M, Holden J (2013) How wetlands affect floods. Wetlands 33: 773-786. https://doi.org/10.1007/s13157-013-0473-2

Adab H, Kanniah KD, Solaimani K (2013) Modeling forest fire risk in the northeast of Iran using remote sensing and GIS techniques. Natural Hazards 65: 1723-1743. https://doi.org/10.1007/s11069-012-0450-8

Agnihotri G, Mohapatra M (2012) Prediction of occurrence of daily summer monsoon precipitation over Karnataka. Meteorological Applications 19(2): 130-139. https://doi.org/10.1002/met.246

Ahern M, Kovats RS, Wilkinson P, Few R, Matthies F (2005) Global health impacts of floods: Epidemiologic evidence. Epidemiologic Reviews 27(1): 36-46. https://doi.org/10.1093/epirev/mxi004

Ahmadlou M, Al-Fugara A, Al-Shabeeb AR, Arora A, Al-Adamat R, Pham QB, Al-Ansari N, Linh NTT, Sajedi H (2021) Flood susceptibility mapping and assessment using a novel deep learning model combining multilayer perceptron and autoencoder neural networks. Journal of Flood Risk Management 14(1). https://doi.org/10.1111/jfr3.12683

Ajin RS, Krishnamurthy RR, Jayaprakash M, Vinod PG (2013) Flood hazard assessment of Vamanapuram river basin, Kerala, India: An approach using remote sensing and GIS techniques. Advances in Applied Science Research 4: 263-274.

Ajin RS, Loghin AM, Vinod PG, Jacob MK (2019) Flood hazard zone mapping in the tropical Achankovil river basin in Kerala: a study using remote sensing data and geographic information system. Journal of Wetlands Biodiversity 9: 45-58.

Ajin RS, Loghin AM, Vinod PG, Jacob MK, Krishnamurthy RR (2016) Landslide susceptible zone mapping using ARS and GIS techniques in selected taluks of Kottayam district, Kerala, India. International Journal of Applied Remote Sensing and GIS 3(1): 16-25.

Ajin RS, Loghin AM, Vinod PG, Menon ARR, Jacob MK (2018) Forest fire risk assessment using geospatial techniques: A study in Mannarkkad forest division of Palakkad district, Kerala, India. ECOTERRA - Journal of Environmental Research and Protection 15(1): 1-9.

Alam A, Bhat MS, Maheen M (2020) Using Landsat satellite data for assessing the land use and land cover change in Kashmir valley. GeoJournal 85: 1529-1543. https://doi.org/10.1007/s10708-019-10037-x

Ali SA, Parvin F, Pham QB, Vojtek M, Vojteková J, Costache R, Linh NTT, Nguyen HQ, Ahmad A, Ghorbani MA (2020) GIS-based comparative assessment of flood susceptibility mapping using hybrid multi-criteria decision-making approach, naïve Bayes tree, bivariate statistics and logistic regression: A case of Topľa basin, Slovakia. Ecological Indicators 117. https://doi.org/10.1016/j.ecolind.2020.106620

Allaire M (2018) Socio-economic impacts of flooding: A review of the empirical literature. Water Security 3: 18-26. https://doi.org/10.1016/j.wasec.2018.09.002

Altin TB, Gökkaya E (2015) Landslide-triggering factors in Korucak sub basin, North Anatolian, Turkey. Procedia Earth and Planetary Science 15: 566-572. https://doi.org/10.1016/j.proeps.2015.08.104

Anis Z, Wissem G, Vali V, Smida H, Mohamed Essghaier G (2019) GIS-based landslide susceptibility mapping using bivariate statistical methods in North-western Tunisia. Open Geosciences 11(1): 708-726. https://doi.org/10.1515/geo-2019-0056

Ayele GT, Tebeje AK, Demissie SS, Belete MA, Jemberrie MA, Teshome WM, Mengistu DT, Teshale EZ (2018) Time series land cover mapping and change detection analysis using geographic information system and remote sensing, Northern Ethiopia. Air, Soil and Water Research. https://doi.org/10.1177/1178622117751603

Ayhan MB (2013) A fuzzy AHP approach for supplier selection problem: A case study in a gear motor company. International Journal of Managing Value and Supply Chains 4(3): 11-23. https://doi.org/10.5121/ijmvsc.2013.4302

Belal AA, El-Ramady HR, Mohamed ES, Saleh AM (2014) Drought risk assessment using remote sensing and GIS techniques. Arabian Journal of Geosciences 7: 35-53. https://doi.org/10.1007/s12517-012-0707-2

Bentekhici N, Bellal SA, Zegrar A (2020) Contribution of remote sensing and GIS to mapping the fire risk of Mediterranean forest case of the forest massif of Tlemcen (North-West Algeria). Natural Hazards 104: 811-831. https://doi.org/10.1007/s11069-020-04191-6

Berhane G, Kebede M, Alfarah N, Hagos E, Grum B, Giday A, Abera T (2020) Landslide susceptibility zonation mapping using GIS-based frequency ratio model with multi-class spatial data-sets in the Adwa-Adigrat mountain chains, northern Ethiopia. Journal of African Earth Sciences 164. https://doi.org/10.1016/j.jafrearsci.2020.103795

Beven KJ, Kirkby MJ (1979) A physically based, variable contributing area model of basin hydrology. Hydrological Sciences Journal 24(1): 43-69. https://doi.org/10.1080/02626667909491834

Bizzi S, Lerner DN (2015) The use of stream power as an indicator of channel sensitivity to erosion and deposition processes. River Research and Applications 31(1): 16-27. https://doi.org/10.1002/rra.2717

Bohorquez P, del Moral-Erencia JD (2017) 100 years of competition between reduction in channel capacity and streamflow during floods in the Guadalquivir river (Southern Spain). Remote Sensing 9(7). https://doi.org/10.3390/rs9070727

Bouamrane A, Derdous O, Dahri N, Tachi SE, Boutebba K, Bouziane MT (2020) A comparison of the analytical hierarchy process and the fuzzy logic approach for flood susceptibility mapping in a semi-arid ungauged basin (Biskra basin: Algeria). International Journal of River Basin Management. https://doi.org/10.1080/15715124.2020.1830786

Brivio PA, Colombo R, Maggi M, Tomasoni R (2002) Integration of remote sensing data and GIS for accurate mapping of flooded areas. International Journal of Remote Sensing 23(3): 429-441. https://doi.org/10.1080/01431160010014729

Buckley JJ (1985) Fuzzy hierarchical analysis. Fuzzy Sets Systems 17(1): 233-247.

Chou SW, Chang, YC (2008) The implementation factors that influence the ERP (Enterprise Resource Planning) benefits. Decision Support Systems 46(1): 149-157.

Danumah JH, Odai SN, Saley BM, Szarzynski J, Thiel M, Kwaku A, Kouame FK, Akpa LY (2016) Flood risk assessment and mapping in Abidjan district using multi-criteria analysis (AHP) model and geoinformation techniques, (cote d'ivoire). Geoenvironmental Disasters 3. https://doi.org/10.1186/s40677-016-0044-y

Das S (2020) Flood susceptibility mapping of the Western Ghat coastal belt using multi-source geospatial data and analytical hierarchy process (AHP). Remote Sensing Applications: Society and Environment 20. https://doi.org/10.1016/j.rsase.2020.100379

Dekrita YA, Yunus R, Citta AB, Yamin M (2019) Integration of balanced scorecard and analytical hierarchy process as a tool for determining the priority of the program strategy: Case study in Dr. Tc. Hillers Maumere hospital. 3rd International Conference on Accounting, Management and Economics 2018 (ICAME 2018),

Advances in Economics, Business and Management Research 92: 71-84. https://dx.doi.org/10.2991/icame-18.2019.8

Dewan AM, Kumamoto T, Nishigaki M (2006) Flood hazard delineation in Greater Dhaka, Bangladesh using an integrated GIS and remote sensing approach. Geocarto International 21(2): 33-38. https://doi.org/10.1080/10106040608542381

Domakinis C, Mouratidis A, Voudouris K, Astaras T, Karypidou MC (2020) Flood susceptibility mapping in Erythropotamos river basin with the aid of Remote Sensing and GIS. AUC Geographica 55(2): 149-164. https://doi.org/10.14712/23361980.2020.11

Dutta D, Kundu A, Patel NR, Saha SK, Siddiqui AR (2015) Assessment of agricultural drought in Rajasthan (India) using remote sensing derived vegetation condition index (VCI) and standardized precipitation index (SPI). The Egyptian Journal of Remote Sensing and Space Science 18(1): 53-63. https://doi.org/10.1016/j.ejrs.2015.03.006

El Morjani ZE, Seif Ennasr M, Elmouden A, Idbraim S, Bouaakaz B, Saad A (2017) Flood hazard mapping and modeling using GIS applied to the Souss river watershed. In: Choukr-Allah R, Ragab R, Bouchaou L, Barceló D (eds) The Souss-Massa river basin, Morocco (The handbook of environmental chemistry 53). Springer, Switzerland, pp 57-93. https://doi.org/10.1007/698_2016_69

Erena SH, Worku H (2018) Flood risk analysis: causes and landscape based mitigation strategies in Dire Dawa city, Ethiopia. Geoenvironmental Disasters 5. https://doi.org/10.1186/s40677-018-0110-8

Fernández DS, Lutz MA (2010) Urban flood hazard zoning in Tucumán Province, Argentina, using GIS and multicriteria decision analysis. Engineering Geology 111(1-4): 90-98. https://doi.org/10.1016/j.enggeo.2009.12.006

Ghosh S, Mistri B (2015) Geographic concerns on flood climate and flood hydrology in monsoon-dominated Damodar river basin, Eastern India. Geography Journal. https://doi.org/10.1155/2015/486740

Gigović L, Pamučar D, Bajić Z, Drobnjak S (2017) Application of GIS-interval rough AHP methodology for flood hazard mapping in urban areas. Water 9(6). https://doi.org/10.3390/w9060360

Government of Kerala (2019) Memorandum: Floods and landslides 2019, Department of Disaster Management, Govt. of Kerala, pp 1-88. Available at https://sdma.kerala.gov.in/disaster-memoranda/

Graf W (1983) Downstream changes in stream power in the Henry Mountains, Utah. Annals of the Association of American Geographers 73(3): 373-387.

Gregory JH, Dukes MD, Jones PH, Miller GL (2006) Effect of urban soil compaction on infiltration rate. Journal of Soil and Water Conservation 61(3): 117-124.

Hillel D (1982) Introduction to Soil Physics. Academic Press, Massachusetts, United States of America.

Ho-Hagemann HTM, Hagemann S, Rockel B (2015) On the role of soil moisture in the generation of heavy rainfall during the Oder flood event in July 1997. Tellus A: Dynamic Meteorology and Oceanography 67(1). https://doi.org/10.3402/tellusa.v67.28661

Hosmer DW, Lemeshow S (2000) Applied logistic regression, Second edition. John Wiley & Sons, Inc., United States of America.

Hunt KMR, Menon A (2020) The 2018 Kerala floods: a climate change perspective. Climate Dynamics 54: 2433-2446. https://doi.org/10.1007/s00382-020-05123-7

Husain M (2012) Geography of India, Third edition. Tata McGraw Hill Education Private Limited, New Delhi, India.

Jaiswal RK, Mukherjee S, Raju KD, Saxena R (2002) Forest fire risk zone mapping from satellite imagery and GIS. International Journal of Applied Earth Observation and Geoinformation 4(1): 1-10. https://doi.org/10.1016/S0303-2434(02)00006-5

James S, Sathian B, van Teijlingen E, Asim M (2018) Outbreak of Leptospirosis in Kerala. Nepal Journal of Epidemiology 8(4): 745-747. https://doi.org/10.3126/nje.v8i4.23876

Jobin SR, Prakash JW (2020) Outbreak of Leptospirosis in Kerala, India after floods: A survey. Plant Archives 20(1): 2560-2562.

Kalantari Z, Nickman A, Lyon SW, Olofsson B, Folkeson L (2014) A method for mapping flood hazard along roads. Journal of Environmental Management 133: 69-77. https://doi.org/10.1016/j.jenvman.2013.11.032

Kaya I, Çolak M, Terzi F (2019) A comprehensive review of fuzzy multi criteria decision making methodologies for energy policy making. Energy Strategy Reviews 24: 207-228. https://doi.org/10.1016/j.esr.2019.03.003

Krishna TM, Ravikumar G, Krishnaveni M (2009) Remote sensing based agricultural drought assessment in Palar basin of Tamil Nadu state, India. Journal of the Indian Society of Remote Sensing 37: 9-20. https://doi.org/10.1007/s12524-009-0008-8

Kumar S, Gupta S (2016) Geospatial approach in mapping soil erodibility using CartoDEM – A case study in hilly watershed of Lower Himalayan range. Journal of Earth System Science 125(7): 1463-1472. https://doi.org/10.1007/s12040-016-0738-2

Kumi-Boateng B, Peprah MS, Larbi EK (2020) The integration of analytical hierarchy process (AHP), fuzzy analytical hierarchy process (FAHP), and Bayesian belief network (BBN) for flood-prone areas identification – A case study of the Greater Accra region, Ghana. Journal of Geomatics 14(2): 100-122.

Legesse G, Suryabhagavan KV (2014) Remote sensing and GIS based agricultural drought assessment in East Shewa Zone, Ethiopia. Tropical Ecology 55: 349-363.

Lin CN (2020) A fuzzy analytic hierarchy process-based analysis of the dynamic sustainable management index in leisure agriculture. Sustainability 12(13). https://doi.org/10.3390/su12135395

Martín-Vide JP, Amarilla M, Zárate FJ (2014) Collapse of the Pilcomayo river. Geomorphology 205: 155-163. https://doi.org/10.1016/j.geomorph.2012.12.007

Merkuryeva G, Merkuryev Y, Sokolov BV, Potryasaev S, Zelentsov VA, Lektauers A (2015) Advanced river flood monitoring, modelling and forecasting. Journal of Computational Science 10: 77-85. https://doi.org/10.1016/j.jocs.2014.10.004

Mersha T, Meten M (2020) GIS-based landslide susceptibility mapping and assessment using bivariate statistical methods in Simada area, northwestern Ethiopia. Geoenvironmental Disasters 7. https://doi.org/10.1186/s40677-020-00155-x

Mishra V, Shah HL (2018) Hydroclimatological perspective of the Kerala flood of 2018. Journal of the Geological Society of India 92: 645-650. https://doi.org/10.1007/s12594-018-1079-3

Moglen GE, Eltahir EAB, Bras RL (1998) On the sensitivity of drainage density to climate change. Water Resources Research 34(4): 855-862.

Moore ID, Gessler PE, Nielsen GA, Peterson GA (1993) Soil attribute prediction using terrain analysis. Soil Science Society of America Journal 57(2): 443-452. https://doi.org/10.2136/sssaj1993.03615995005700020058x

Moore ID, Grayson RB, Ladson AR (1991) Digital terrain modelling: A review of hydrological, geomorphological, and biological applications. Hydrological Processes 5(1): 3-30. https://doi.org/10.1002/hyp.3360050103

Msabi MM, Makonyo M (2021) Flood susceptibility mapping using GIS and multi-criteria decision analysis: A case of Dodoma region, central Tanzania. Remote Sensing Applications: Society and Environment 21. https://doi.org/10.1016/j.rsase.2020.100445

Muthumanickam D, Kannan P, Kumaraperumal R, Natarajan S, Sivasamy R, Poongodi C (2011) Drought assessment and monitoring through remote sensing and GIS in western tracts of Tamil Nadu, India, International Journal of Remote Sensing 32(18): 5157-5176. https://doi.org/10.1080/01431161.2010.494642

Orimoloye IR, Ololade OO, Mazinyo SP, Kalumba AM, Ekundayo OY, Busayo ET, Akinsanola AA, Nel W (2019) Spatial assessment of drought severity in Cape Town area, South Africa. Heliyon 5(7). https://doi.org/10.1016/j.heliyon.2019.e02148

Panda PK, Sahoo S (2015) Modelling of floodplain using recent technology. European Journal of Advances in Engineering and Technology 2(7): 23-28.

Paquette J, Lowry J (2012) Flood hazard modelling and risk assessment in the Nadi River Basin, Fiji, using GIS and MCDA. The South Pacific Journal of Natural and Applied Sciences 30(1): 33-43. https://doi.org/10.1071/SP12003

Parajuli A, Gautam AP, Sharma SP, Bhujel KB, Sharma G, Thapa PB, Bist BS, Poudel S (2020) Forest fire risk mapping using GIS and remote sensing in two major landscapes of Nepal. Geomatics, Natural Hazards and Risk 11(1): 2569-2586. https://doi.org/10.1080/19475705.2020.1853251

Petersen MS (2001) Impacts of flash floods. In: Gruntfest E, Handmer J (eds) Coping with flash floods. NATO science series (Series 2. Environmental security), vol 77. Springer, Dordrecht. https://doi.org/10.1007/978-94-010-0918-8_2

Prachansri S (2017) Analysis of soil and land cover parameters for flood hazard assessment; A case study of the Nam Chun watershed, Phetchabun, Thailand. International Institute for Geo-Information Science and Earth Observation, Enschede, The Netherlands. Available from https://webapps.itc.utwente.nl/librarywww/papers_2007/msc/aes/prachansri.pdf

Pratomo RA, Jetten V, Alkema D (2016) Rural flash-flood behaviour in Gouyave watershed, Grenada, Caribbean Island. Geoplanning Journal of Geomatics Planning 3(2): 161-170. https://doi.org/10.14710/geoplanning.3.2.161-170

Putra MSD, Andryana S, Fauziah, Gunaryati A (2018) Applications of fuzzy multicriteria decision making to complex engineering problems. Advances in Fuzzy Systems. https://doi.org/10.1155/2018/9094380

Rahman M, Ningsheng C, Islam MM, Dewan A, Iqbal J, Washakh RMA, Shufeng T (2019) Flood susceptibility assessment in Bangladesh using machine learning and multi-criteria decision analysis. Earth Systems and Environment 3: 585-601. https://doi.org/10.1007/s41748-019-00123-y

Saaty TL (1980) The analytic hierarchy process: planning, priority setting, resource allocation (Decision making series). McGraw Hill, New York, United States of America.

Samanta S, Pal DK, Palsamanta B (2018) Flood susceptibility analysis through remote sensing, GIS and frequency ratio model. Applied Water Science 8. https://doi.org/10.1007/s13201-018-0710-1

Sarkar D, Mondal P (2020) Flood vulnerability mapping using frequency ratio (FR) model: a case study on Kulik river basin, Indo-Bangladesh Barind region. Applied Water Science 10. https://doi.org/10.1007/s13201-019-1102-x

Setiawan I, Mahmud AR, Mansor S, Shariff ARM, Nuruddin AA (2004) GIS-grid-based and multi-criteria analysis for identifying and mapping peat swamp forest fire hazard in Pahang, Malaysia. Disaster Prevention and Management 13(5): 379-386. https://doi.org/10.1108/09653560410568507

Shahabi H, Hashim M (2015) Landslide susceptibility mapping using GIS-based statistical models and Remote sensing data in tropical environment. Scientific Reports 5. https://doi.org/10.1038/srep09899

Shahfahad, Mourya M, Kumari B, Tayyab M, Paarcha A, Asif, Rahman A (2020) Indices based assessment of built-up density and urban expansion of fast-growing Surat city using multi-temporal Landsat data sets. GeoJournal. https://doi.org/10.1007/s10708-020-10148-w

Shen L, Li C (2010) Water body extraction from Landsat ETM+ imagery using adaboost algorithm. 2010 18th International Conference on Geoinformatics: 1-4. https://doi.org/10.1109/GEOINFORMATICS.2010.5567762

Smiley SL, Hambati H (2019) Impacts of flooding on drinking water access in Dar es Salaam, Tanzania: implications for the sustainable development goals. Journal of Water, Sanitation and Hygiene for Development 9(2): 392-396. https://doi.org/10.2166/washdev.2019.168

Souissi D, Zouhri L, Hammami S, Msaddek MH, Zghibi A, Dlala M (2020) GIS-based MCDM – AHP modeling for flood susceptibility mapping of arid areas, southeastern Tunisia. Geocarto International 35(9): 991-1017. https://doi.org/10.1080/10106049.2019.1566405

Swain KC, Singha C, Nayak L (2020) Flood susceptibility mapping through the GIS-AHP technique using the cloud. ISPRS International Journal of Geo-Information 9(12). https://doi.org/10.3390/ijgi9120720

Tehrany MS, Shabani F, Jebur MN, Hong H, Chen W, Xie X (2017) GIS-based spatial prediction of flood prone areas using standalone frequency ratio, logistic regression, weight of evidence and their ensemble techniques. Geomatics, Natural Hazards and Risk 8(2): 1538-1561. https://doi.org/10.1080/19475705.2017.1362038

Tehrany MS, Pradhan B, Mansor S, Ahmad N (2015) Flood susceptibility assessment using GIS-based support vector machine model with different kernel types. CATENA 125: 91-101. https://doi.org/10.1016/j.catena.2014.10.017

Tehrany MS, Kumar L, Jebur MN, Shabani F (2019) Evaluating the application of the statistical index method in flood susceptibility mapping and its comparison with frequency ratio and logistic regression methods. Geomatics, Natural Hazards and Risk 10(1): 79-101. https://doi.org/10.1080/19475705.2018.1506509

Tiryaki M, Karaca O (2018) Flood susceptibility mapping using GIS and multicriteria decision analysis: Saricay-Çanakkale (Turkey). Arabian Journal of Geosciences 11. https://doi.org/10.1007/s12517-018-3675-3

Ullah K, Zhang J (2020) GIS-based flood hazard mapping using relative frequency ratio method: A case study of Panjkora River Basin, eastern Hindu Kush, Pakistan. PLoS ONE 15(3). https://doi.org/10.1371/journal.pone.0229153

Vojtek M, Vojteková J (2019) Flood Susceptibility Mapping on a National Scale in Slovakia Using the Analytical Hierarchy Process. Water 11(2). https://doi.org/10.3390/w11020364

Yong B, Ren LL, Hong Y, Gourley JJ, Chen X, Zhang YJ, Yang XL, Zhang ZX, Wang WG (2012) A novel multiple flow direction algorithm for computing the topographic wetness index. Hydrology Research 43(1-2): 135-145. https://doi.org/10.2166/nh.2011.115

Zha Y, Gao J, Ni S (2003) Use of normalized difference built-up index in automatically mapping urban areas from TM imagery. International Journal of Remote Sensing 24(3): 583-594. https://doi.org/10.1080/01431160304987

Zou KH, O'Malley AJ, Mauri L (2007) Receiver-Operating Characteristic analysis for evaluating diagnostic tests and predictive models. Circulation 115(5): 654-657. https://doi.org/10.1161/CIRCULATIONAHA.105.594929

Figures

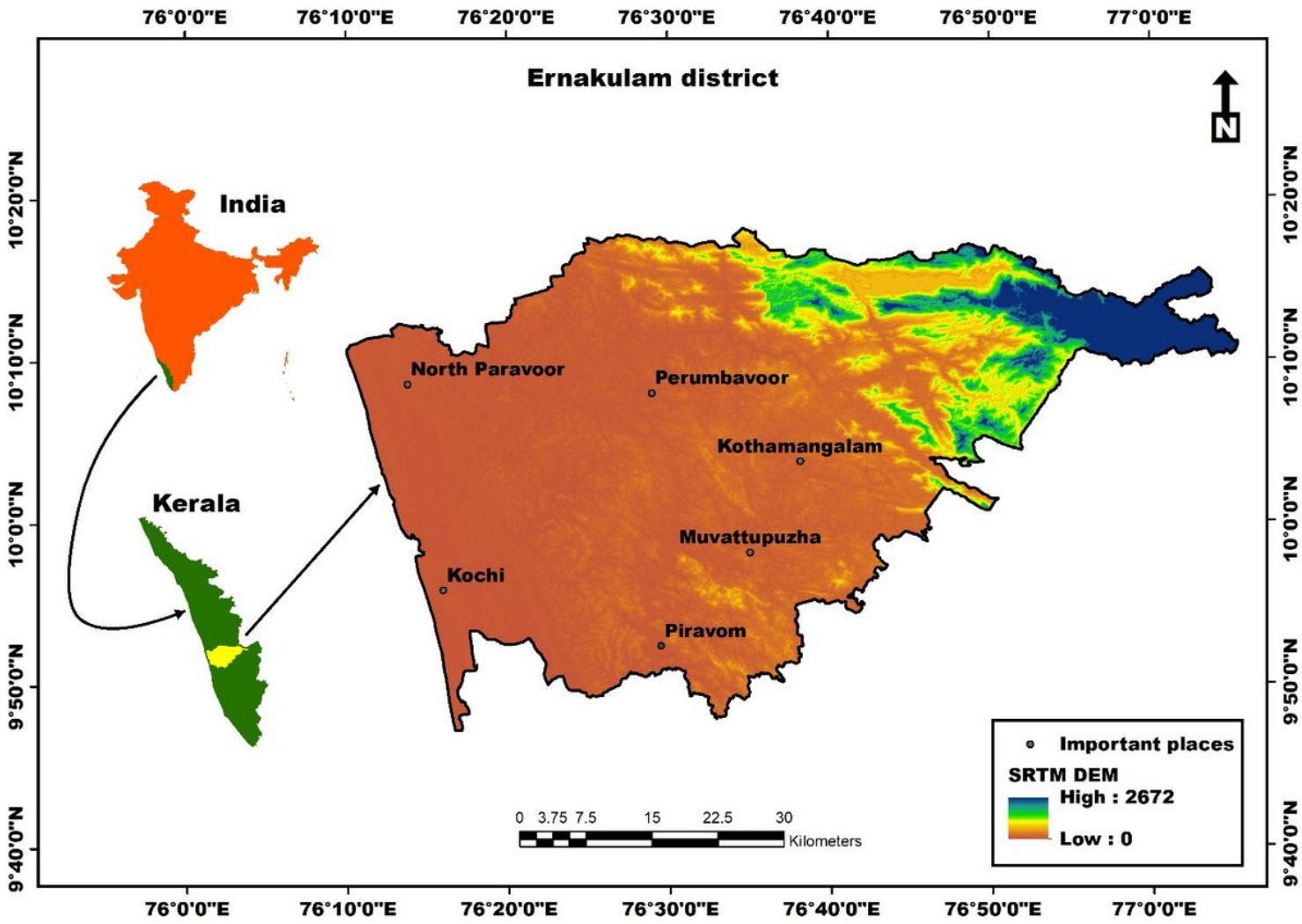

Figure 1

Location of the study area

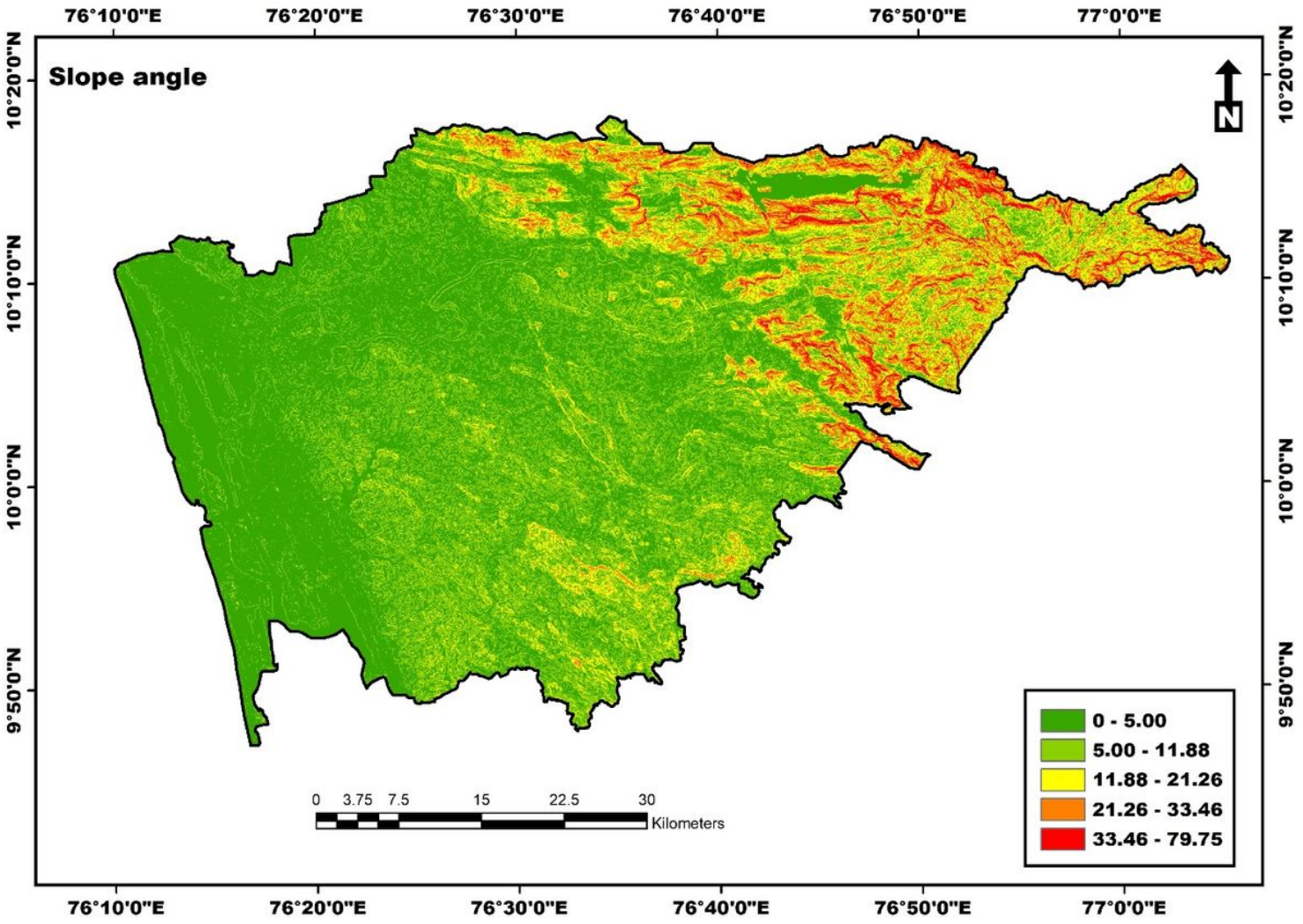

Figure 2

Slope

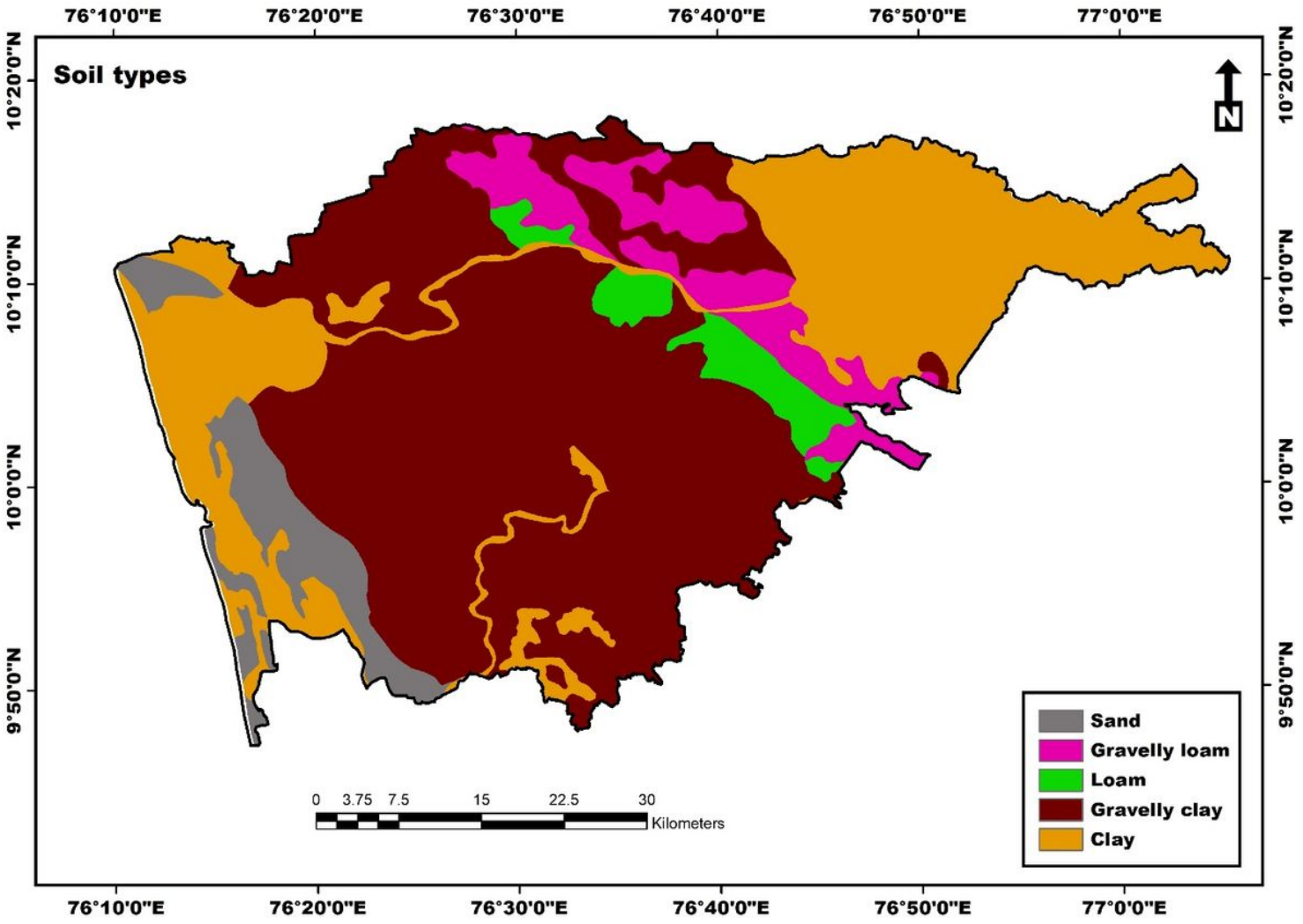

Figure 3

Soil types

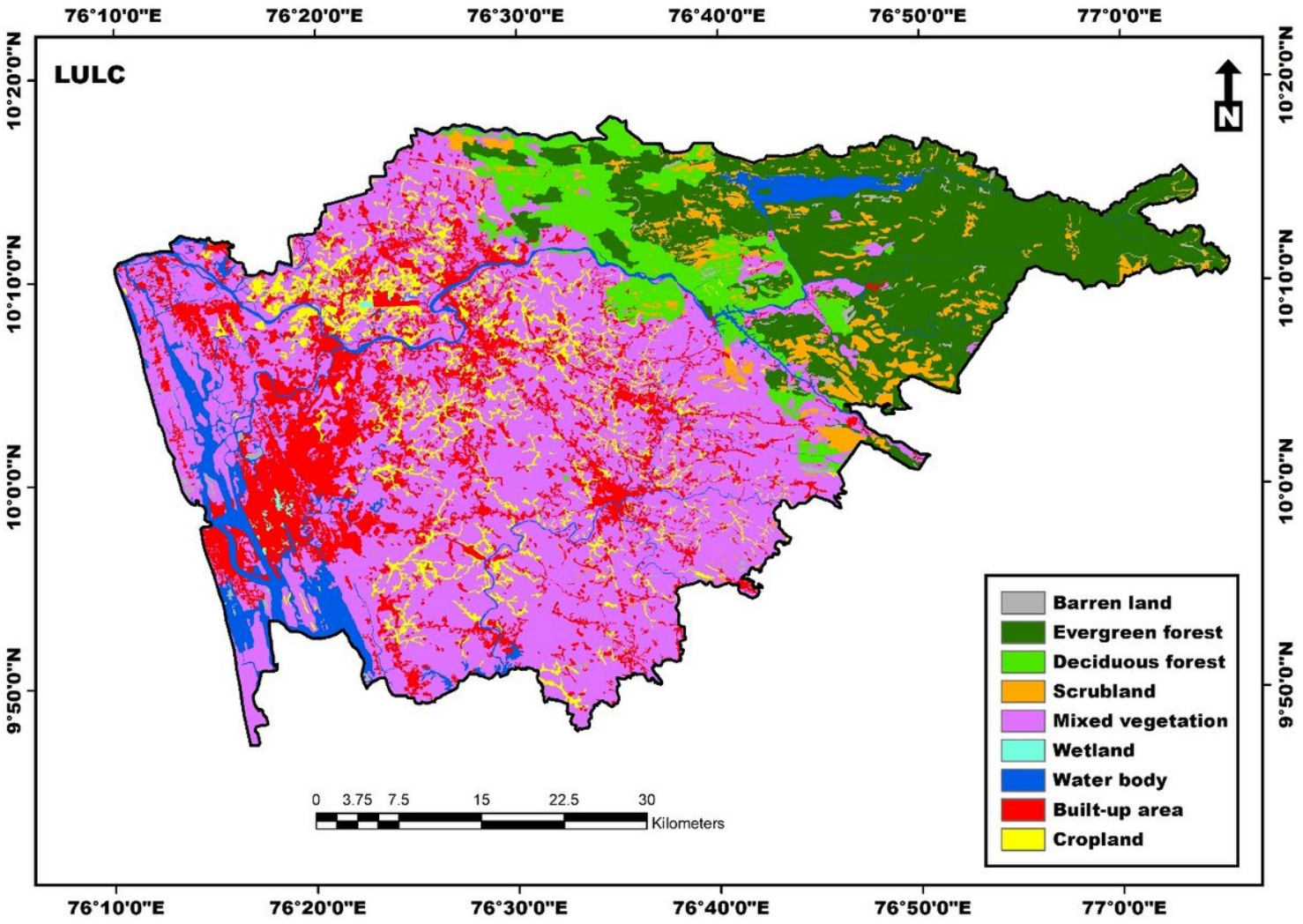

Figure 4

LULC

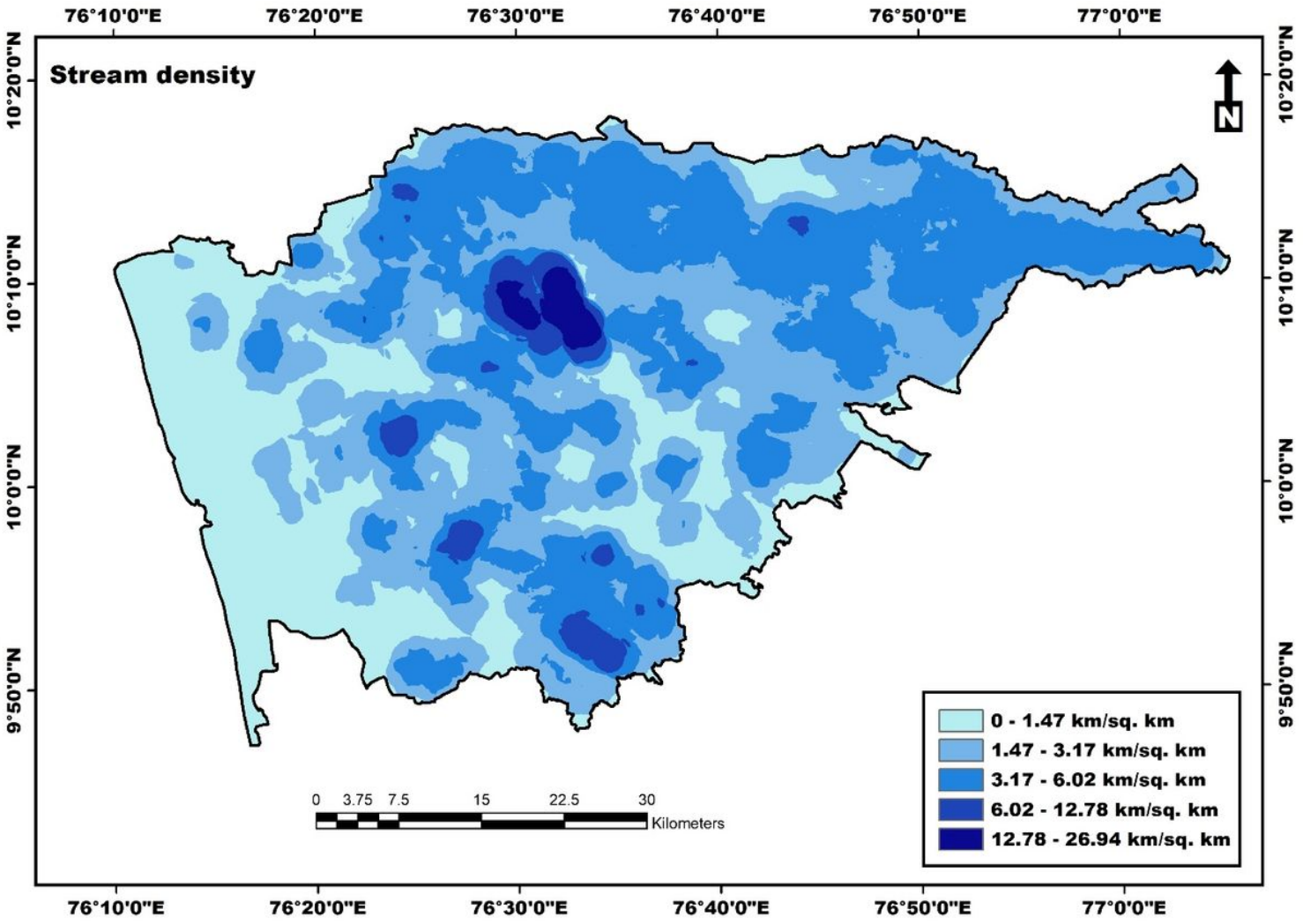

Figure 5

Stream Density

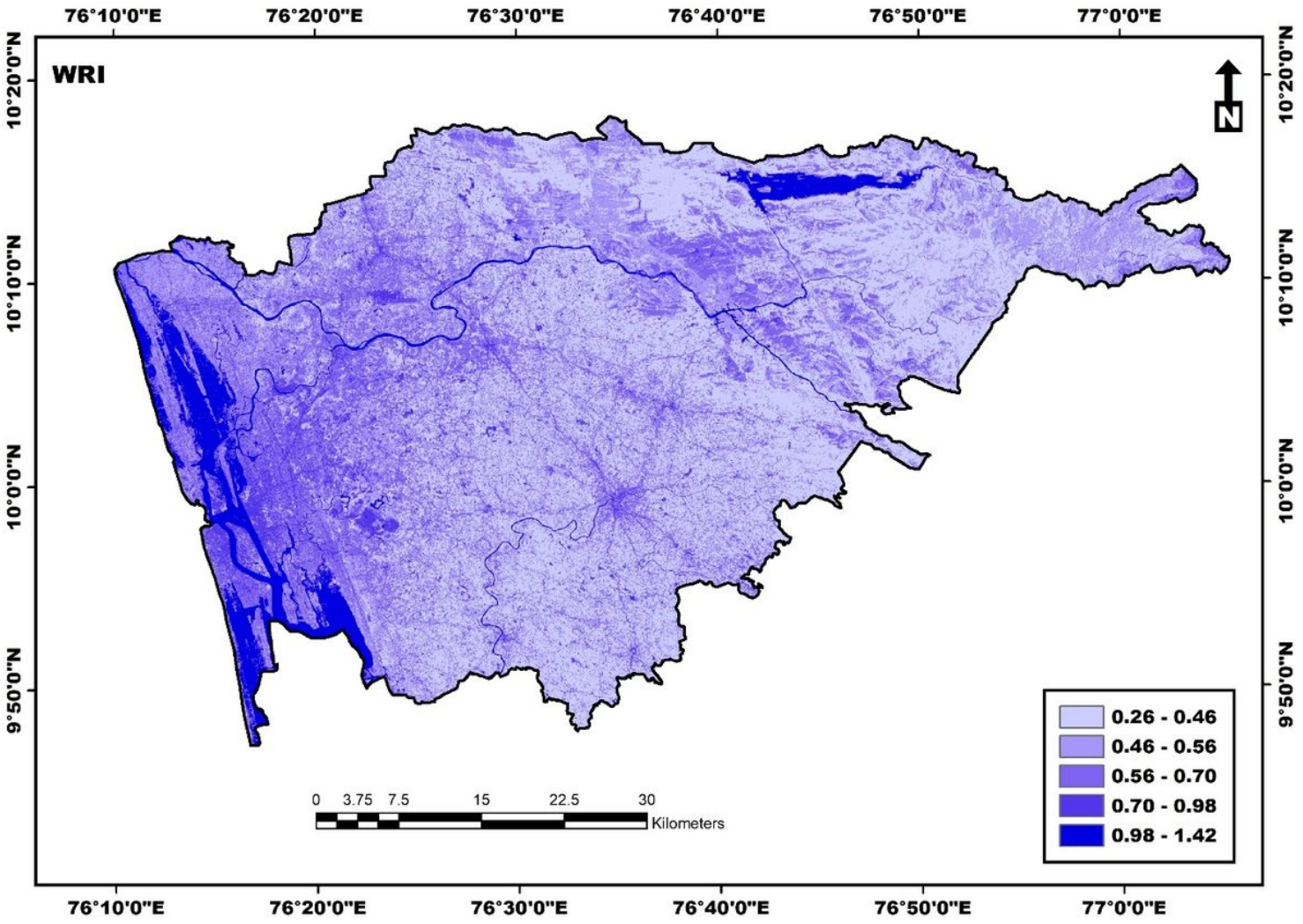

Figure 6

Water ratio index

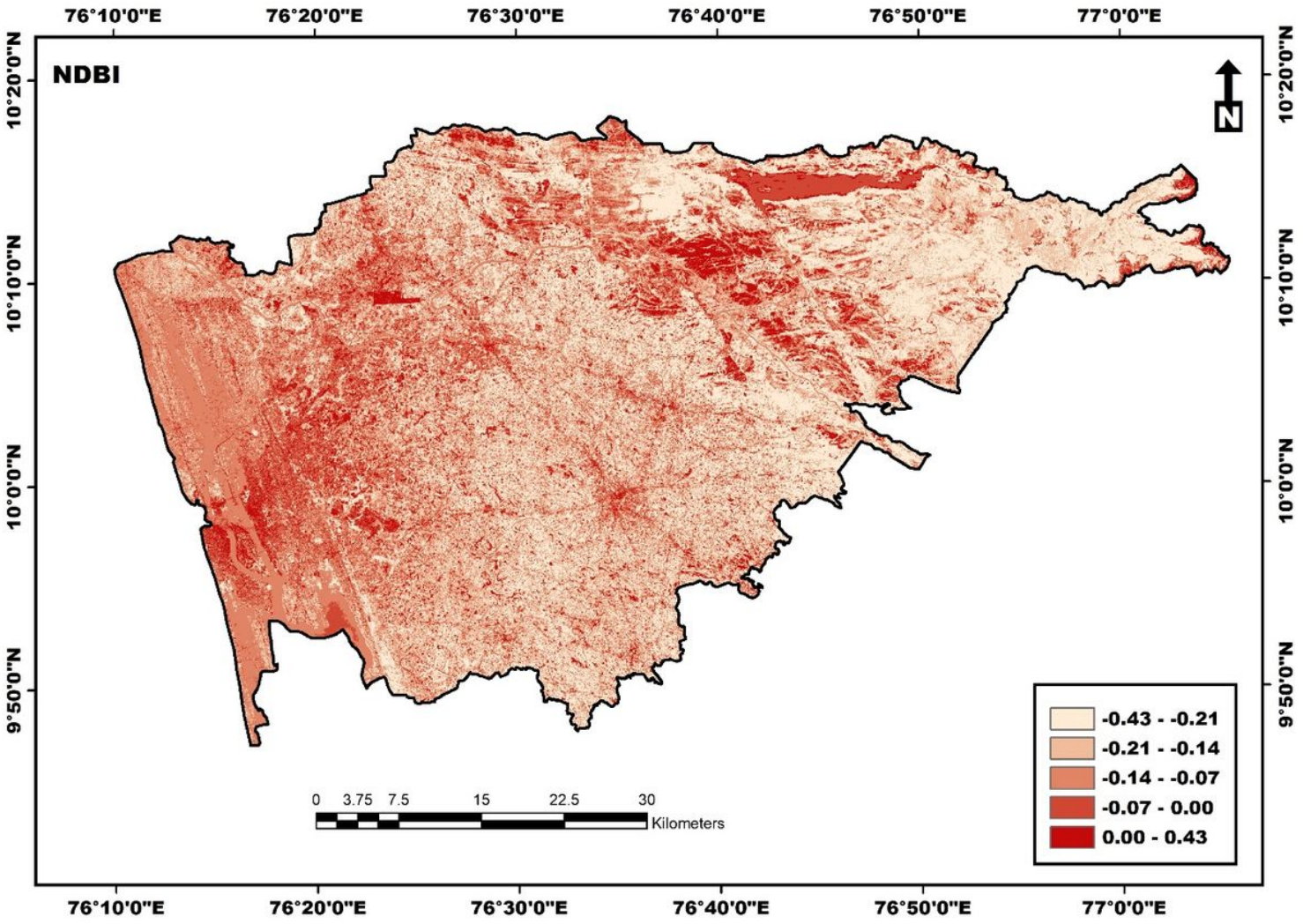

Figure 7

Normalized difference built-up index

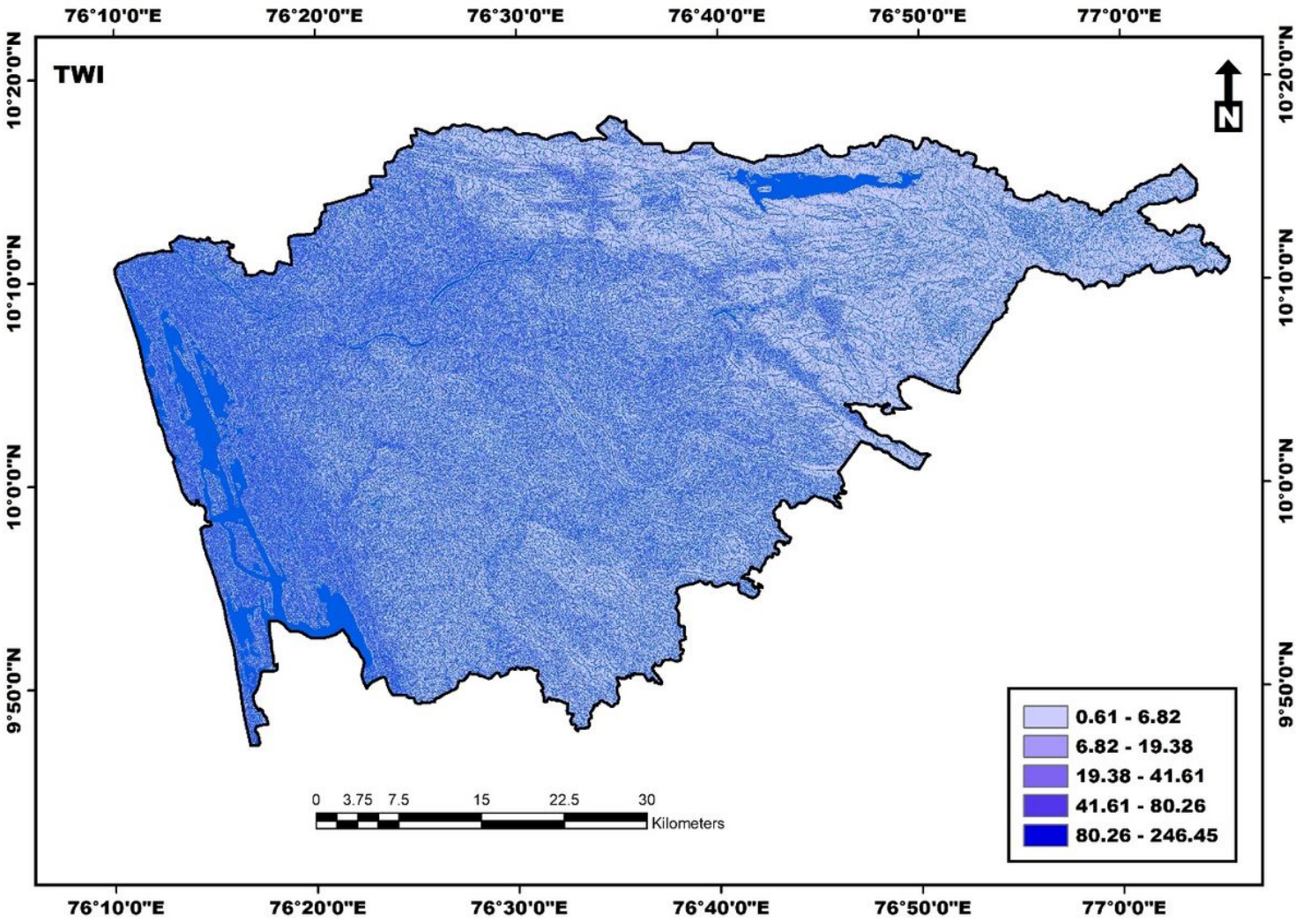

Figure 8

Topographic wetness index

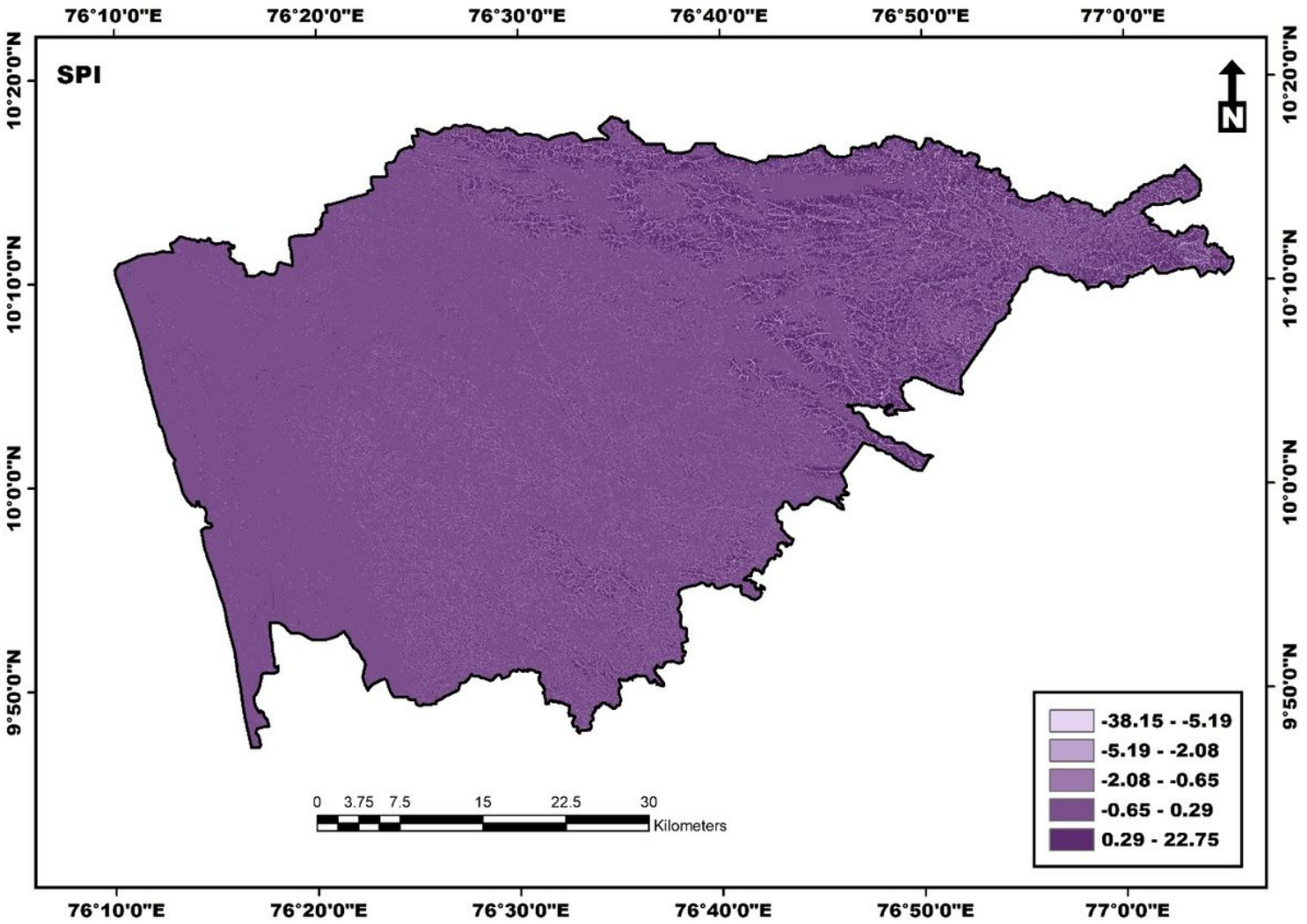

Figure 9

Stream power index

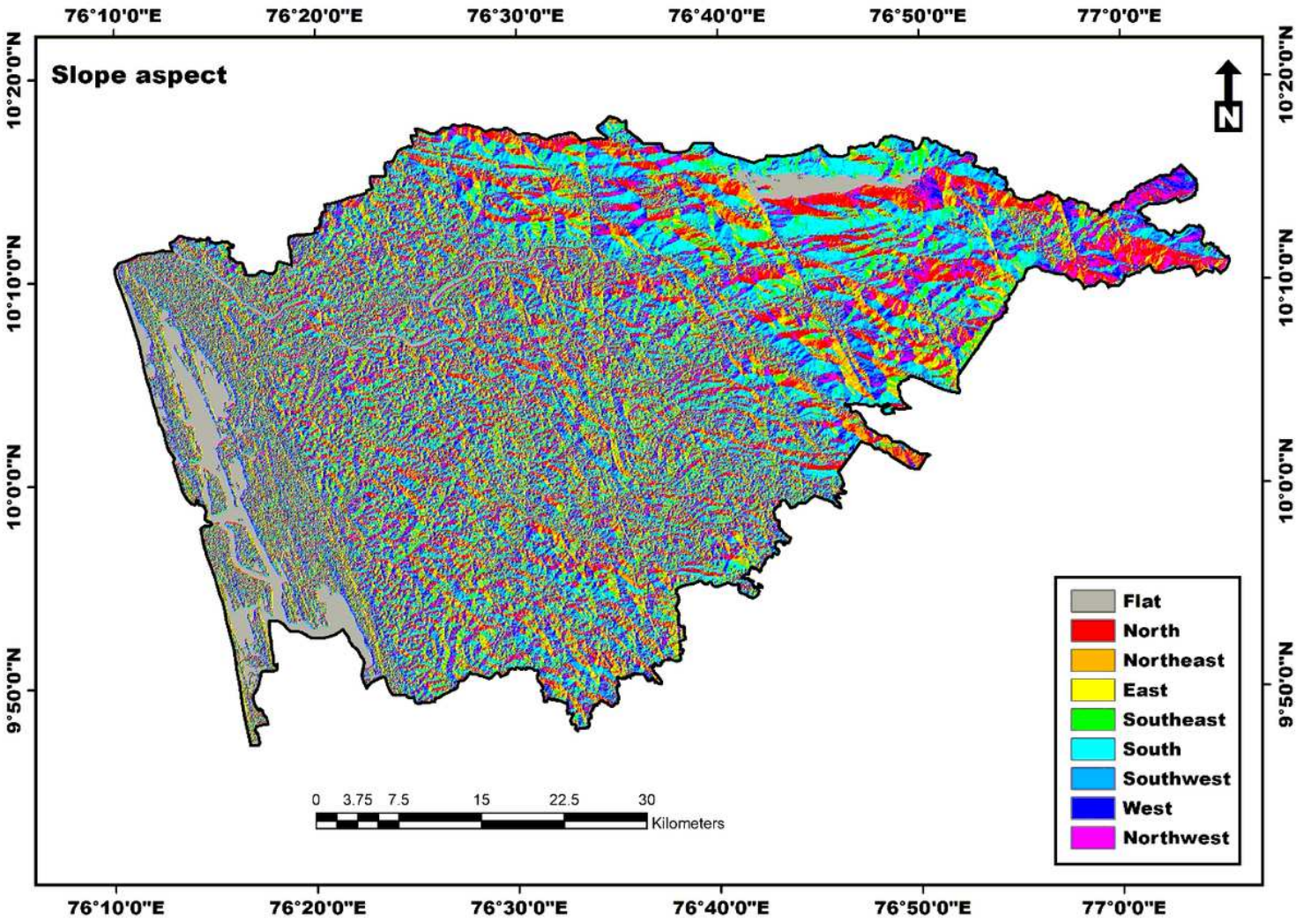

Figure 10

Slope Aspect

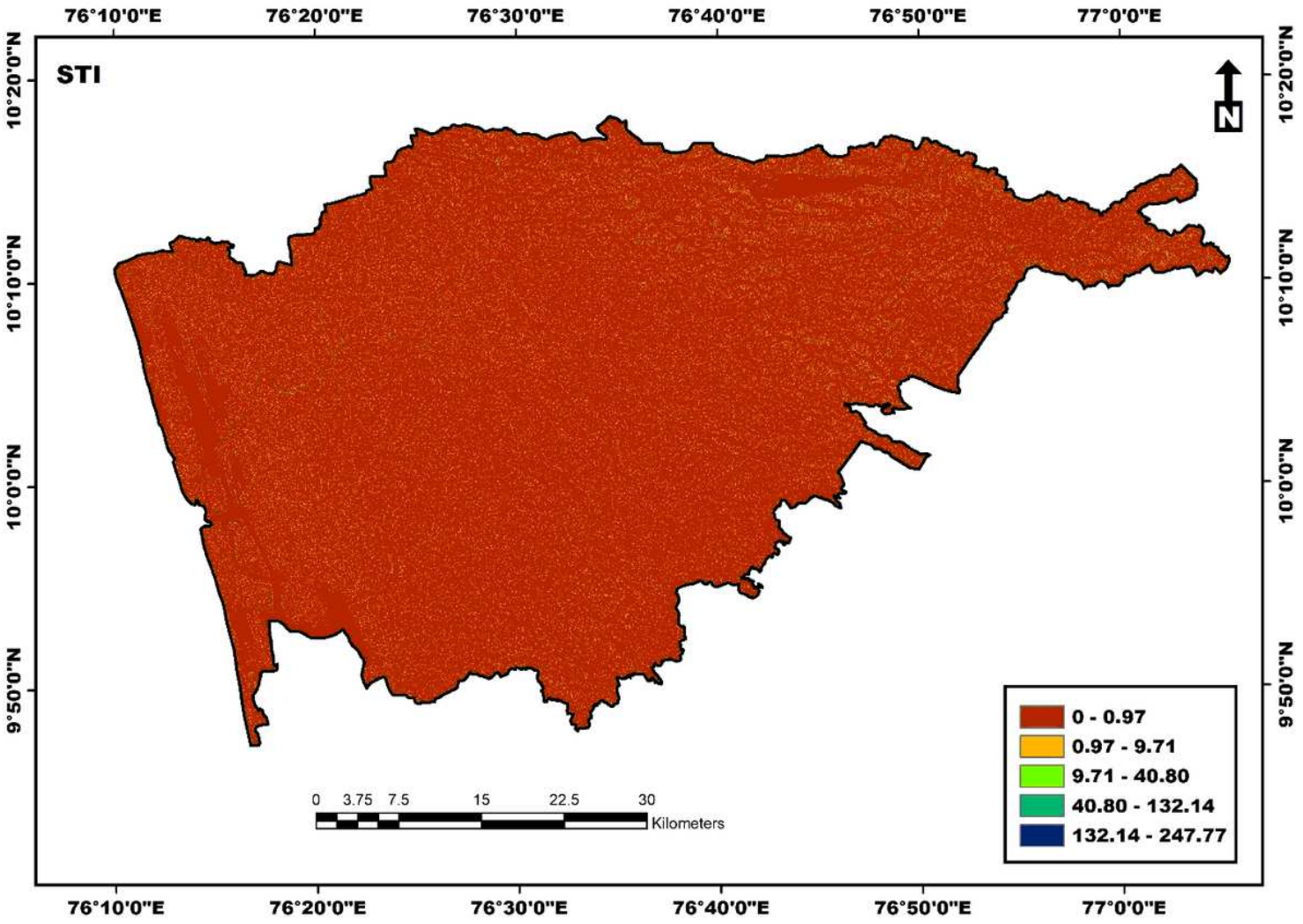

Figure 11

Sediment transport index

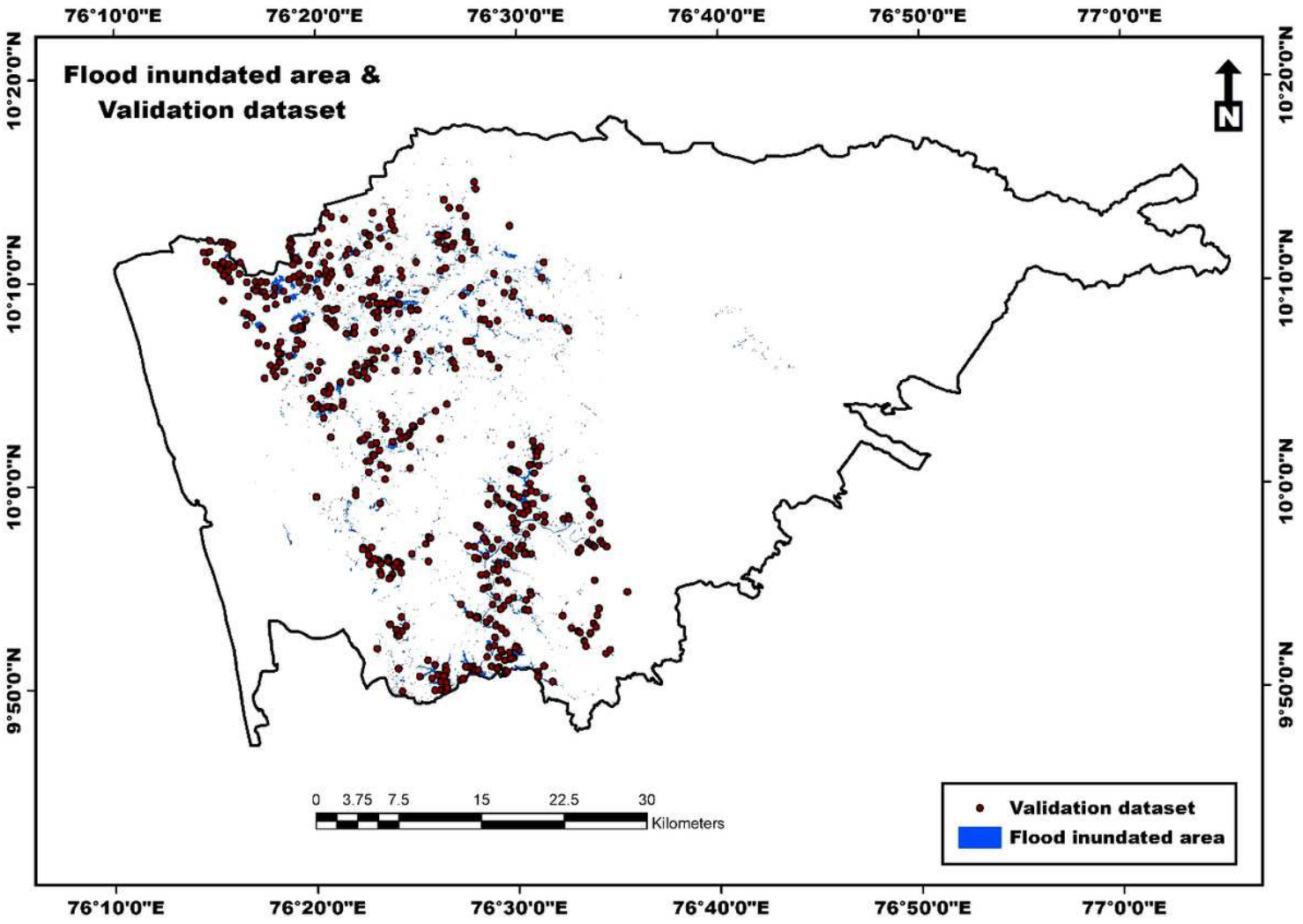

Figure 12

Flood inundation area

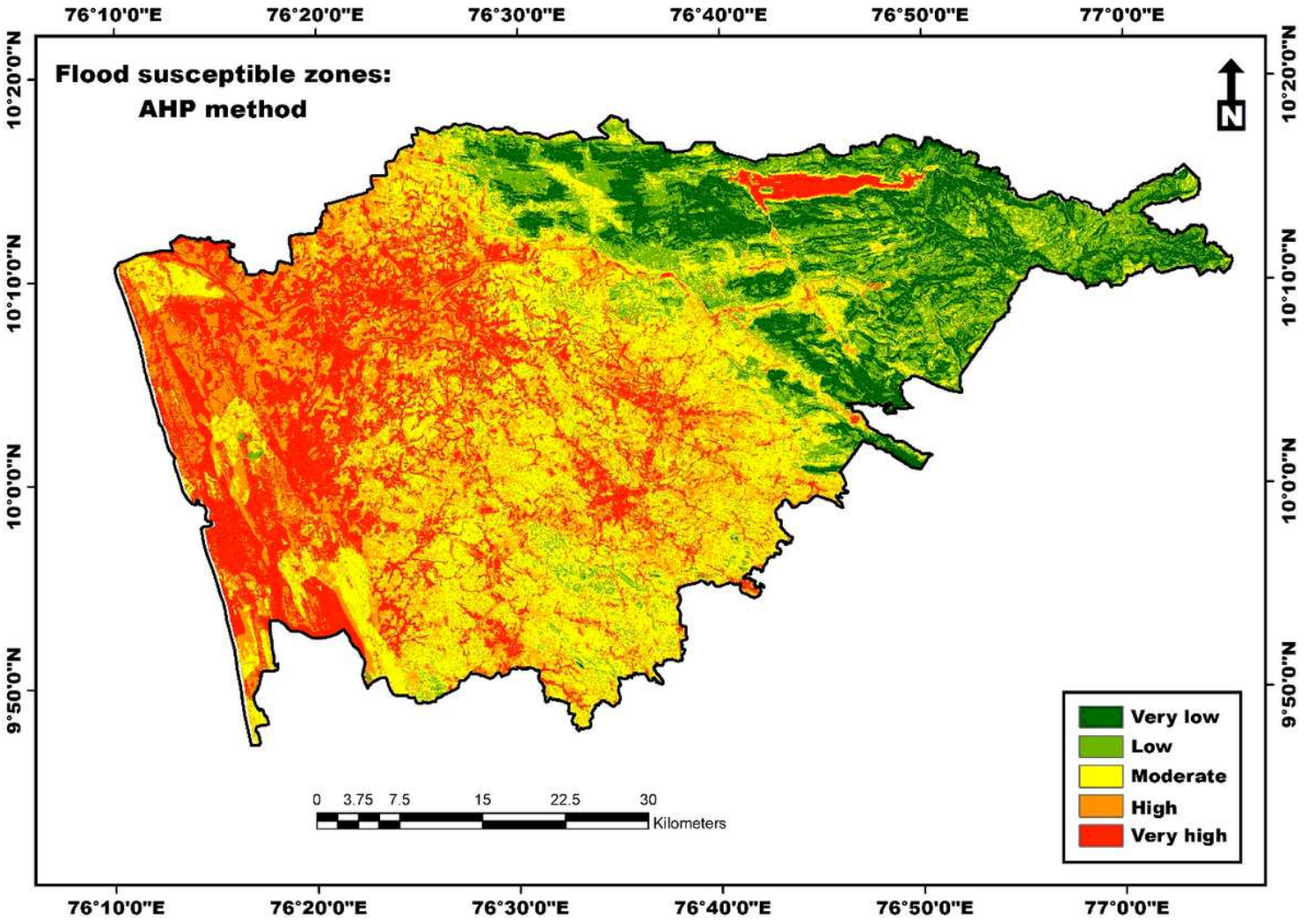

Figure 13

Flood susceptible zones: AHP method

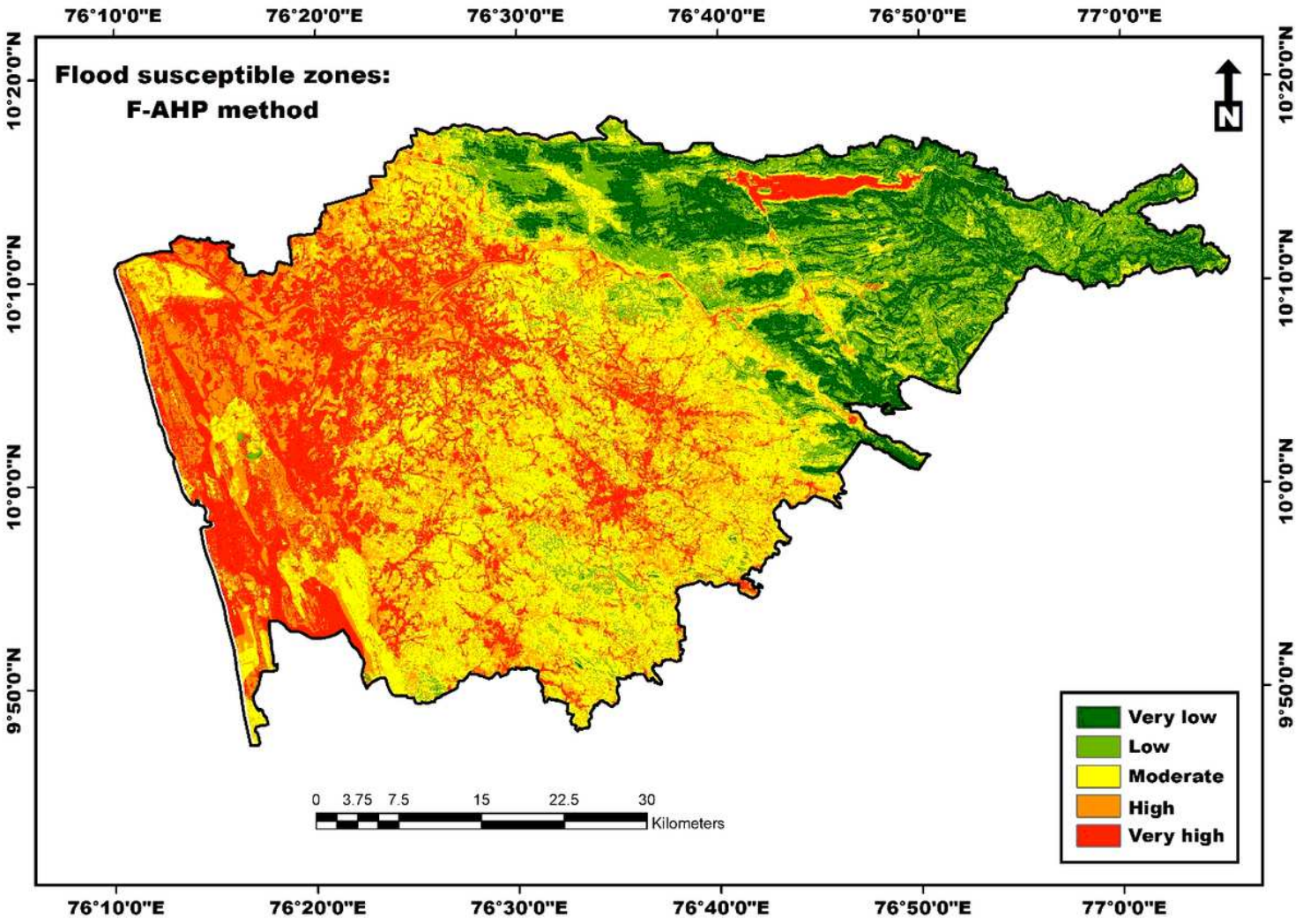

Figure 14

Flood susceptible zones: F-AHP method

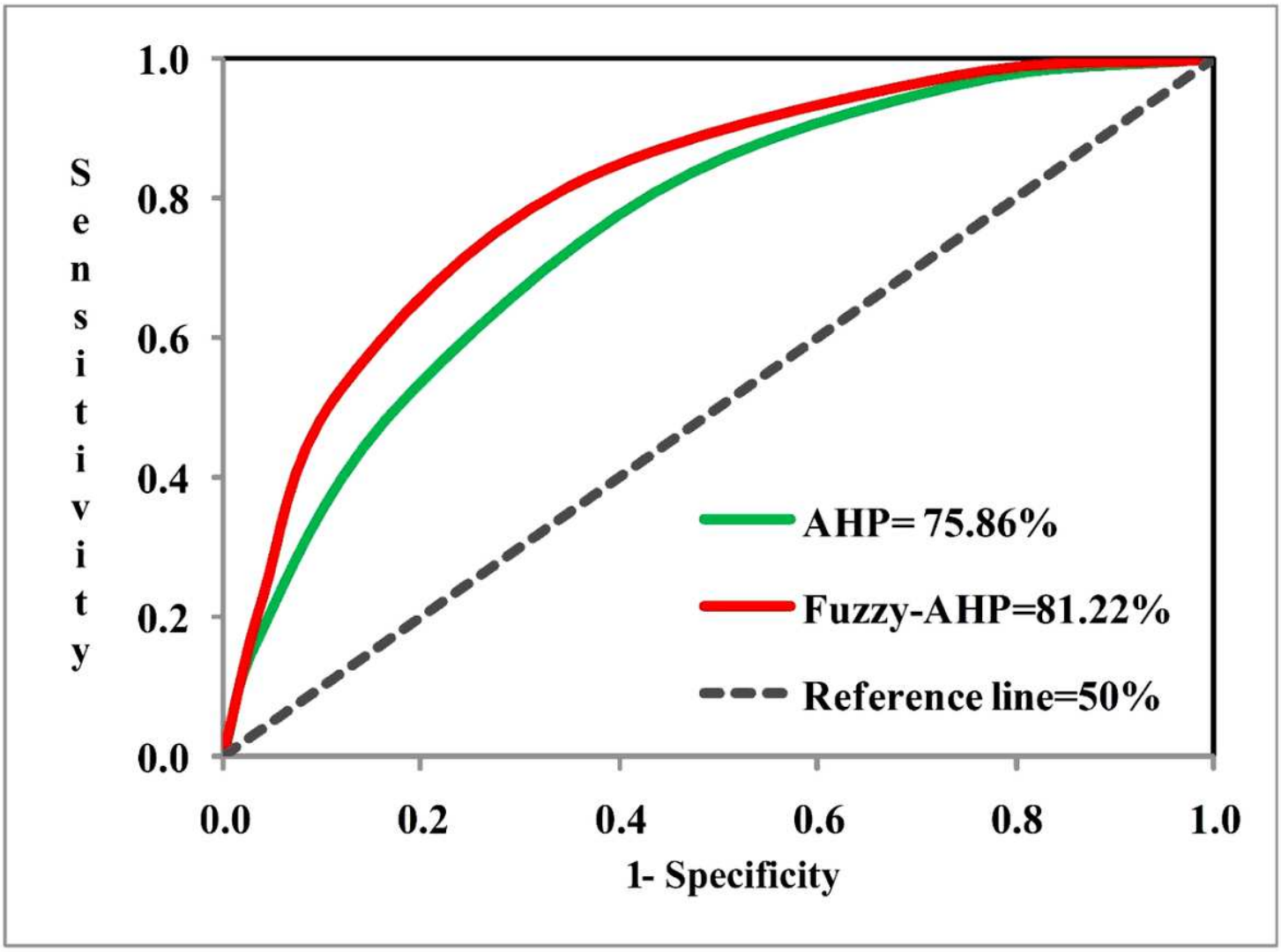

Figure 15

The ROC curves

Supplementary Files

This is a list of supplementary files associated with this preprint. Click to download.

- ManuscriptTables.docx